applied sciences

MDPI

Article

Experimental Study on Backflow Patterns Induced by a Bilateral Groin Pair with Different Spacing

Cuiping Kuang [1], Yuhua Zheng [1,*], Jie Gu [2,*], Qingping Zou [3] and Xuejian Han [1]

[1] College of Civil Engineering, Tongji University, Shanghai 200092, China; cpkuang@tongji.edu.cn (C.K.); hanxuejian11@tongji.edu.cn (X.H.)
[2] College of Marine Ecology and Environment, Shanghai Ocean University, Shanghai 201306, China
[3] The Lyell Centre for Earth and Marine Science and Technology, Institute for Infrastructure and Environment, Heriot-Watt University, Edinburgh EH14 4AS, UK; q.zou@hw.ac.uk
* Correspondence: yhzheng@tongji.edu.cn (Y.Z.); jgu@shou.edu.cn (J.G.); Tel.: +86-21-6598-3916 (Y.Z.)

Abstract: Groins are one of the popular manmade structures to modify the hydraulic flow and sediment response in river training. The spacing between groins is a critical consideration to balance the channel-depth and the cost of construction, which is generally determined by the backflow formed downstream from groins. A series of experiments were conducted using Particle Image Velocimetry (PIV) to observe the influence of groin spacing on the backflow pattern of two bilateral groins. The spacing between groins has significant effect on the behavior of the large-scale recirculation cell behind groins. The magnitude of the wake flow induced by a groin was similar to that induced by another groin on the other side, but the flow direction is opposite. The spanwise velocity near the groin tip dictates the recirculation zone width behind the groins due to the strong links between the spanwise velocity and the contraction ratio of channel cross-sections between groins. Based on previous studies and present experimental results, quantitative empirical relationships are proposed to calculate the recirculation zone length behind groins alternately placed at different spacing along riverbanks. This study provides better understanding and a robust formula to assess the backflow extent of alternate groins and identify the optimum groins array configuration.

Keywords: groin; backflow; spacing; PIV

Citation: Kuang, C.; Zheng, Y.; Gu, J.; Zou, Q.; Han, X. Experimental Study on Backflow Patterns Induced by a Bilateral Groin Pair with Different Spacing. *Appl. Sci.* **2021**, *11*, 1486. https://doi.org/10.3390/app11041486

Academic Editor: N. C. Markatos
Received: 18 January 2021
Accepted: 3 February 2021
Published: 6 February 2021

1. Introduction

Groins, also termed spur dikes, have been used widely to protect coastlines and riverbanks from scour and erosion for centuries. They are typically built perpendicularly or at an oblique angle to the bank so that the flow is kept away from the bank [1]. Installing the groins, the laterally confined flow attains a sufficiently high velocity to rectify a navigable river [2]. Due to the blockage effect of the groin, a complex three-dimensional turbulent flow pattern is generated near the structure, resulting in local high velocity-gradient and sediment movement [3]. The flow field in vicinity of groins is a visual indicator of the turbulent flow characteristic and plays a key role in the understanding of hydrodynamics induced by the groin [4,5]. The emerged and impermeable groin is the most common type of groin used in river regulation. The flow field around such a kind of groin can be divided into two subzones due to flow separation from the groin tip: the recirculation zone with a large-scale vortex downstream of the groin and the main stream with contraction and diffusion by the protrusion of the groin (see Figure 1 for detail).

Previous studies have examined the two-dimensional (2D) flow fields around a single groin, the simplest layout, to interpret the mechanism of groin-induced turbulent flow. Most scholars focus on the flow separation from the groin tip [6], back water upstream of the groin [7], dead-water zones in the mixing layer [8], water surface oscillation [9] and the recirculation zone downstream [10,11], as shown in Figure 1. Among issues above, the large-scale recirculation zone of the groin downstream is the hottest topic

discussed due to its key role on the local scour near the structure. The earliest report on the recirculation zone of a thin plate groin was from Francis et al. [12], which presented the structure of the recirculation zone behind the groin and preliminarily investigated the average length and maximum width of the recirculation zone but lacked flow measurement. Rajaratnam and Nwachukwu [13] further experimentally observed the velocity profiles near a thin-plate groin and the recirculation zone downstream. They stated that the length of this recirculation is about 12 the times groin length. Subsequently, Schmidt et al. [14], Ettema and Muste [3], and Duan [15] also conducted a series of physical experiments to simulate recirculating flow varied by different impact factors, i.e., Froude number, approaching velocity and model scale. Their experimental data show that the downstream recirculation length varied from 7 to 16.6 times the length of the groin and suggested that downstream channel training is the key in controlling the recirculation length in natural rivers. These early experimental investigations gave a robust basis for the follow-up study of the recirculation zone induced by a groin-like structure, in particular providing validated data for numerical simulation. Considerable efforts have been devoted to numerical simulation of flow around a single groin with the rapid development of computation technology, presenting more detailed information regarding flow field structure around a single groin [16–22].

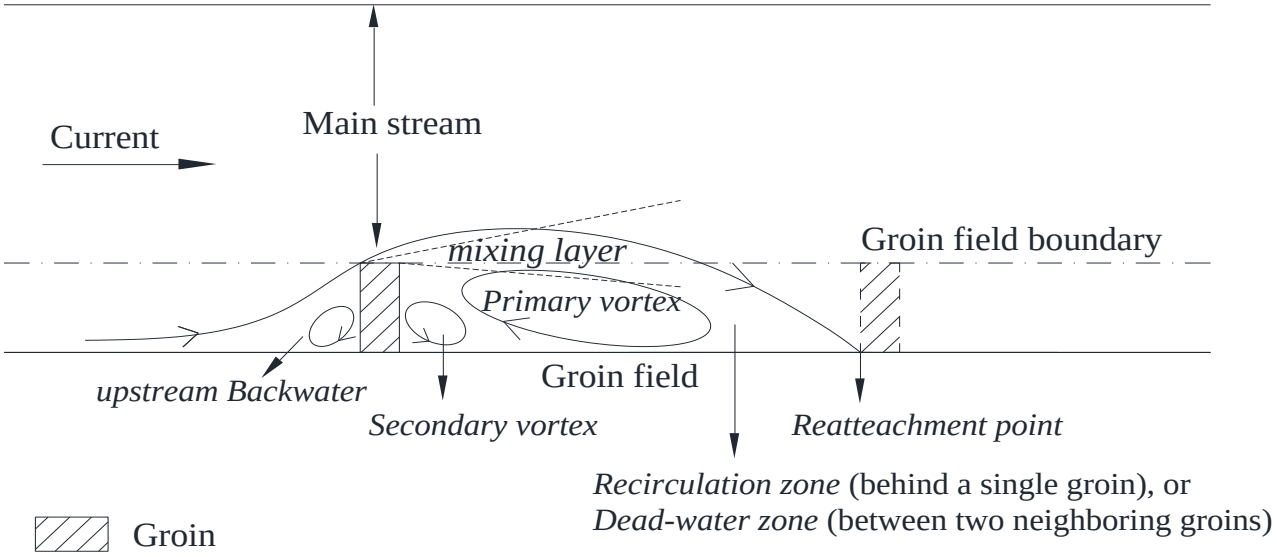

Figure 1. Schematic sketch of flow separation from a groin (Top view).

The flow within the groin field is virtually stagnant and has a permanent open connection with the main stream, resulting in a continuous exchange of mass and momentum between the groin field and main stream [23]. Using the planar velocity measurement with Particle Image Velocimetry (PIV), Weitbrecht and Jirka [24] conducted an experimental work of the flow patterns around two groins and the mass exchange processes between the recirculation zone and the main stream. The exchange process was found to be governed by the 2D flow structure generated at the groin tip, which grows in the horizontal direction mainly between two groins because the flow is very shallow. Based on flume experiments and field measurements, Sukhodolov et al. [25] found that the recirculating flow patterns in the groin fields depend mainly on the ratio between groin length and groin field length. The aspect ratio of 0.5 is the critical value at which the flow pattern changes from one-vortex to two-vortex in the groin fields. Subsequently, more details regarding vortex flow in groin fields were experimentally investigated by Uijttewaal [26]. By increasing the distance between groins further, the flow pattern on the downstream side of the groin field changes while, on the upstream side, the primary and secondary vortices remain qualitatively the same [26]. More flow details near river groins were further experimentally investigated by

Yossef and de Vriend [27] for emergent and submerged groins. The flow circulation within the emerged groin field is largely driven by the main stream via momentum exchange through the interfacial mixing layer, while the flow in the submerged groin field does not show the same circulation pattern as that in the emerged groin field.

A three-dimensional (3D) view of the flow and turbulent structures is necessary for better understanding the hydrodynamics and particular features of groin-induced flow patterns, particularly concerning the shallow flow associated with low-land rivers [28]. The shallow water depth implies that the horizontal distribution of flow velocities is strongly influenced by the local depth, curvature bed roughness, and the presence of obstacles such as groins. Due to the complexities, the 3D flow in shallow fluids is predicted generally by high-resolution experiment instruments and validated numerical models for large temporal and spatial scales. Using Stereoscopic Particle Image Velocimetry (SPIV), Akkermans et al. [29] measured the horizontal flow velocities around a dipolar vortex generated by a single magnet with pulsed forcing in a shallow fluid layer. The flow exhibits significant 3D features from the patches of downward flow in the vortex cores. Following that, Cieślik et al. [30] investigated the interaction of a shallow-layer vortex dipolar with a lateral wall, and observed that the influence of the wall on the vertical motion inside the dipolar vortex becomes stronger with decreasing water depths via SPIV measurement and numerical simulation. Van Heijst and Clercx [31] reviewed the research work on complicated vortices evolving in shallow fluid layers, and suggested the importance of vertical secondary flows on the surface of primary horizontal motion. Furthermore, Akkermans et al. [32] noticed that the discrepancy of the 3D vortex structure occurred possibly in two-layer and single-layer fluids, and substantiated that 3D vortex structures and their evolution are resembled in both fluids via experimental and numerical simulations.

The influence of a single groin is apparently limited in altering the geometry or flow dynamics of the river channel. In actual practice, groins exert influences on the river system usually in the form of groups, i.e., groin groups, to systematically reshape the river channel. The spatial layout of a groin group is an important factor to realign the river channel and improve the navigation condition, including ipsilateral and bilateral layouts. The ipsilateral layout is several groins deployed on one side in order to regulate the riverbank or coastline. Based on laboratory experiments, McCoy et al. [33], Ahmed et al. [34] studied the flow patterns around an ipsilateral groin pair, focusing on the impact of groin length and distance between groins. Their results indicated that the effective distance between two groins ranges from three to four times the groin length. Uijttewaal [10] examined the flow patterns induced by groin groups with different types, i.e., permeable, impermeable and inclined crest groins, and chiefly observed the vortex shedding and recirculation in the groin field. Installing more groins may prolong the regulating length of the river and cause more a complicated turbulent flow pattern, but this is difficult to measure via laboratory experiment. Employing a numerical model validated by experimental data, the complex recirculating flow inside multiple groins field was successfully captured by McCoy et al. [35], Fang et al. [36], Koutrouveli et al. [37] and Ning et al. [38]. The simulated results show that the center of the downstream recirculation zone moves towards the groin as groin length increases, and the recirculation zone between groins increased with the spacing between two neighboring groins.

Contrary to the ipsilateral layout, groin groups constructed on both sides of a river is a so-called bilateral layout. The bilateral layout of groin groups is generally performed in two forms, i.e., the alternate layout and symmetrical layout, which depends on the relative spacing between groins on both sides. The spacing between groins is a crucial consideration to retain an appropriate channel depth and cost-effective construction. The open-channel flow with groins in the alternate layout was experimentally investigated by Gu and Ikeda [39]. The experimental results show that the spacing between groins has a significant effect on the location of the reattachment point and maximum velocity downstream, leading to change the scale of the recirculation zone formed behind groins.

Further, Cao et al. [40] proposed the spacing threshold of two adjacent groins, which is the spacing when the lateral distribution of velocities adjacent to two groin sections becomes coincides, and compared the velocity distribution of two groins with the ipsilateral layout and alternate layout via numerical simulation. It shows that the spacing threshold of alternate groins is smaller than that of ipsilateral groins. Following that, a contrastive analysis between the hydraulic performances of groins placed ipsilaterally and alternately was carried out by Krishna et al. [41], focusing on water-level fluctuation, velocity distribution and bed patterns around groins. From the results, the alternate arrangement of groins showed a greater increase in water levels and velocities upstream. In terms of flow field characteristic of symmetrical groins, the recirculation zone width induced by groins is highly sensitive to the length of groins, especially the length of the groin placed in middle [42]. Both the recirculation width and length of symmetrical groins at downstream increased with decrease in the cross-section of the main flow, and the average recirculation width and length were 0.4 and 8 times the groin length, respectively [43].

The alternate groins layout was widely used on training large rivers, such as the Mississippi River [44–46], Rhine River [47–49], Yellow River [50,51] and Yangtze River [52–54]. Due to the asymmetric layout, there were significant differences in flow properties between ipsilateral groins and alternate groins. According to previous research [55,56], the extension of the horizontal vortex downstream of a groin can be used as a criterion for selecting the suitable spacing between groins. In spite of all this extensive research, it is still difficult to make a direct estimation of the backflow scope behind groins deployed at both riverbanks. For instance, even for a single groin, the surrounding 3-D turbulent flow change is very complex, not to mention the accumulative interaction with the integrated groin group in a natural river system. Moreover, some questions remain to be answered: how do the backflows generated by alternate groins affect each other? Is there a critical spacing between groins that maximizes or minimizes the respective recirculation zones behind groins? How do they differ from each other in the velocity distribution?

To answer these questions, further research is needed to investigate the backflow interaction mechanism of bilateral groins. From these perspectives, a groin pair, i.e., the smallest unit of a groin group, was adopted to study the river training and regulating effect of the groin group via a series of laboratory flume experiments. The novelties of this study include: (1) two bilateral groins with various spacing were experimentally investigated for their backflow pattern, which was first characterized by the variation process of backflow scale by critical spacing; (2) the quantitative relations of the recirculation zone length and spacing between bilateral groins were established, indicating the influence mechanism of the opposite groin on backflow behavior; (3) spanwise velocity located at the shear layer zone near the groin tip was determined to play a leading role in the width of the downstream recirculation zone; (4) the vorticity distribution with different spacing between groins was calculated and compared with the variation trend of backflow length.

The paper is organized as follows: the experimental setup and measurement technique are introduced in Section 2; the experimental results of a groin pair with various spacing are presented in Section 3, including horizontal flow patterns, velocity along the cross-section through the groin tip, and vorticity distribution; the effect of backflow patterns of Groin B on the recirculation zone behind Groin A, formulas of recirculation length behind a single groin and alternating groins are discussed in Section 4; finally, the conclusions are summarized in Section 5.

2. Material and Methods

2.1. Experimental Set-Up and Test Conditions

The experiments were carried out in the recirculating current flume of the Hydrodynamic Laboratory at Shanghai Ocean University. The current flume is 6.0 m long, 0.45 m wide and 0.55 m deep, as shown in Figure 2. The flow rate ranges from 0.1 to 100 m^3/h. The flume sidewalls and bottom are transparent tempered glass with metal frames to facilitate PIV measurements. The effect of bottom friction is negligible due to the smooth

glass surface. Honeycomb steel plates are installed at the inlet and outlet to minimize eddy currents. A tailgate at the outlet of the flume is used to retain the flow depth. The longitudinal slope of the flume is 0. In present experiment, the discharge and depth of the flow were constant. The inlet discharge was controlled by a computer. The water depth was adjusted using a butterfly tailgate located at the downstream outlet of the flume to maintain the flow depth constant. In present experiment, inlet discharge was set to 25 m^3/h and water depth was set at 0.137 m to keep the groin just emerged. The Reynold number is approximately 366,273.

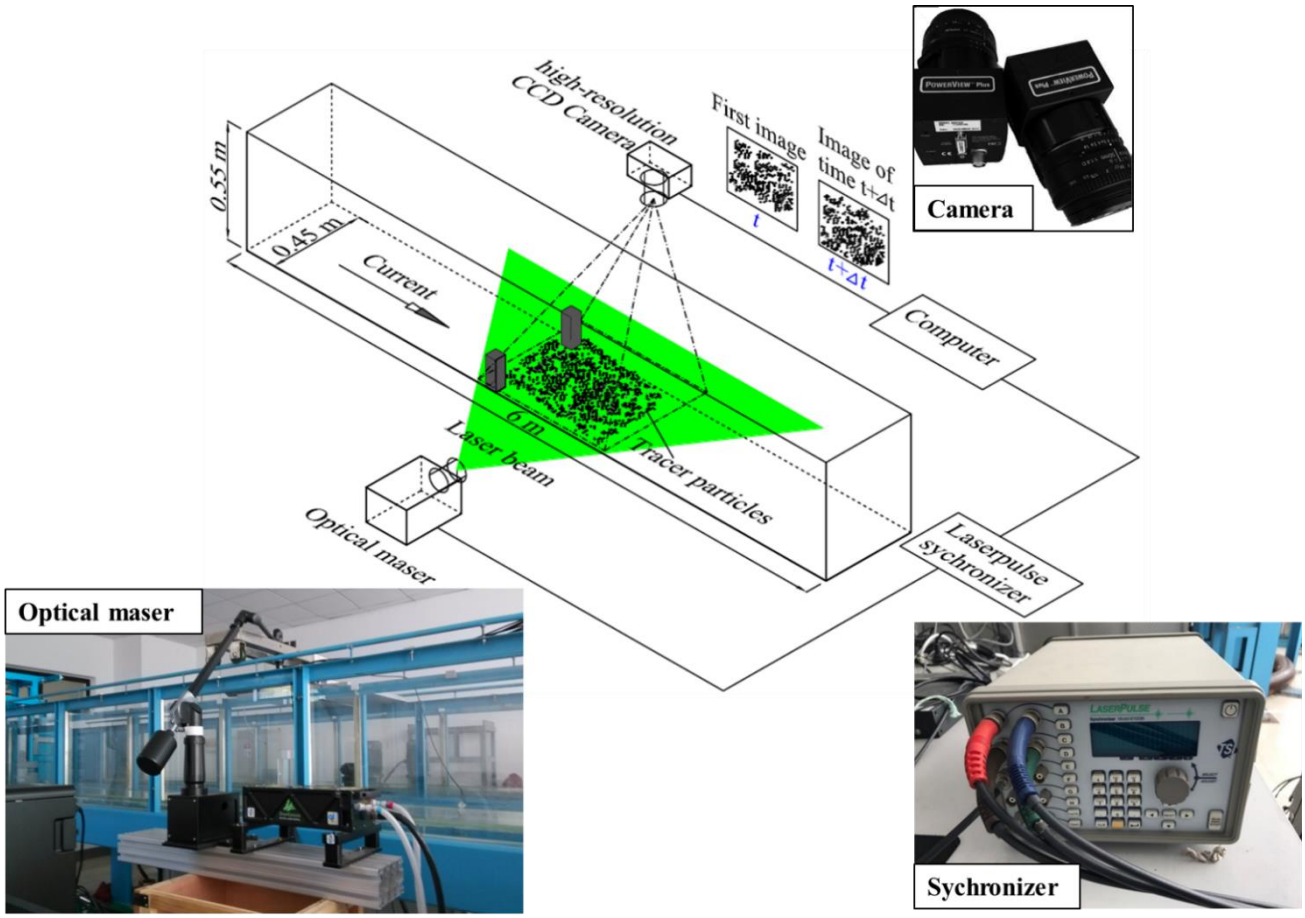

Figure 2. The diagram of flume and Particle Image Velocimetry (PIV) test stand with two symmetrical groins (black rectangular blocks).

Two identical groin models with a dimension of 0.05 m (length) × 0.05 m (width) × 0.15 m (height) were composed of plexiglass and installed on both vertical walls of the flume. The structure length was less than 1/3 of the flume width; therefore, they were taken as short groins. The two groins were labelled Groin A and B. Groin A was fixed and Groin B could be moved on the opposite bank to create a variety of array configurations. For example, by moving groin B along the flume side wall upstream or downstream, the streamwise spacing (x) between two groins was changed to form a variety of alternate layouts ($x \neq 0$). When the two groins were placed transverse parallel at both banks, a symmetrical layout ($x = 0$) was created. A schematic diagram of two groins with various positions for Groin B is shown in Figure 3. During the experiments, the inlet flow rate, the water depth at the tailgate and the position of Groin A remained unchanged.

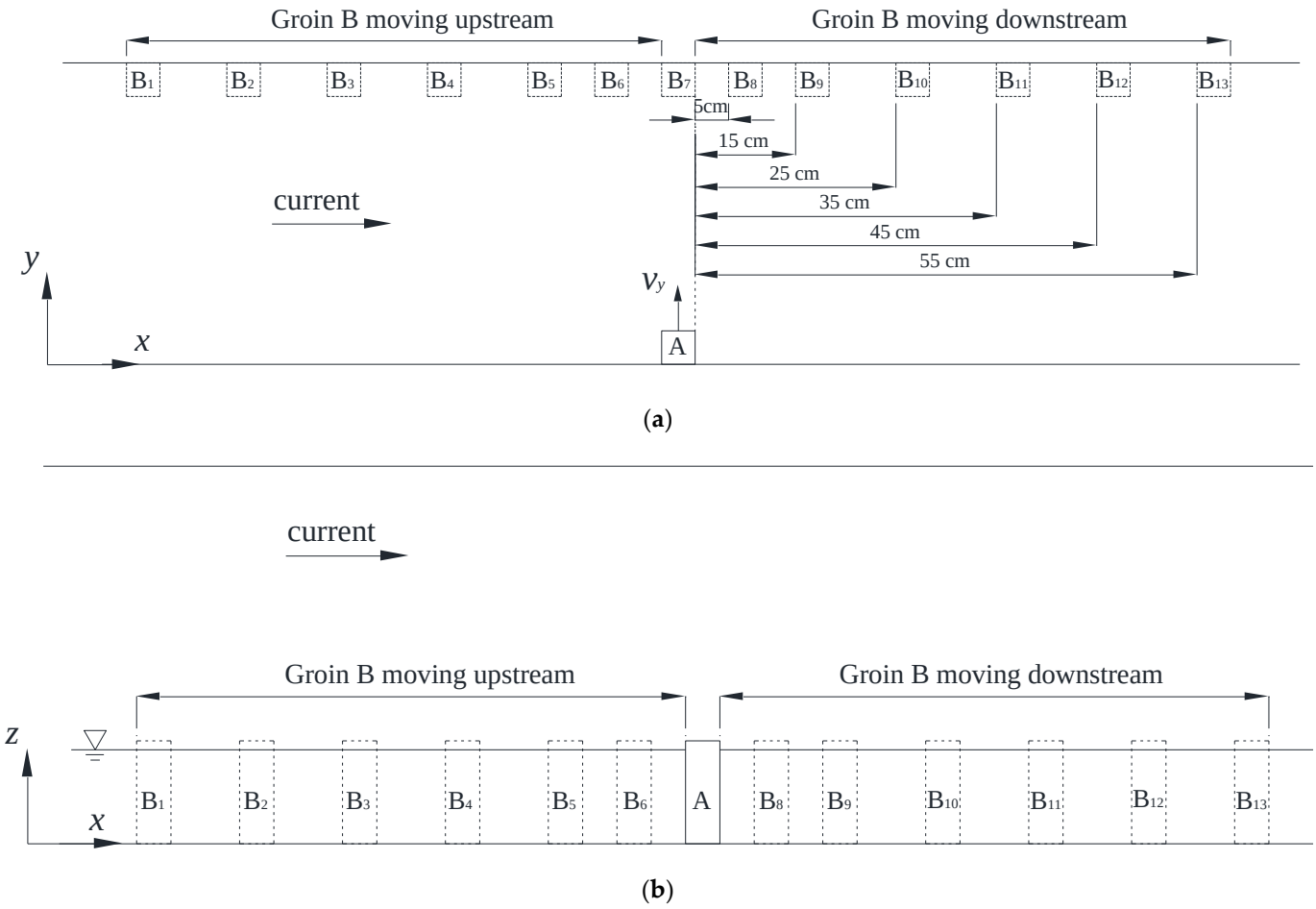

Figure 3. Different groin configuration scenarios. (**a**) Top view; (**b**) side view.

2.2. Particle Image Velocimetry (PIV) Measurements

The flow velocity was measured using a two-dimensional PIV system (TSI, USA), which is a whole-flow-field and non-intrusive laser optical measurement technique for research and diagnostics into flow. It provides instantaneous velocity vector measurements in a cross-section of the flow. The PIV system mainly includes tracer particles, a laser generator, image acquisition, synchronizer and image-processing software, see Figure 2 for detail. PIV systems measure velocity by determining particle displacement over a precisely selected time using a double-pulsed laser technique. A laser light sheet illuminates a plane in the flow, and the positions of particles (naturally present or added to the flow to have a sufficient number of tracers) in that plane are recorded using a digital camera. A short time (micro or milliseconds) later, a second pulse illuminates the same plane, creating a second set of particle images. From these sets of images, PIV analysis algorithms obtain the particle displacements for the imaged region to give the velocity information at thousands of locations—quickly, easily, reliably. Flow properties such as the vorticity and strain rates are obtained. Mean velocity, turbulence intensity, and higher order statistics are also obtained.

In recent years, given the marked improved accuracy and visualization of PIV measurements, PIV has become a popular tool for examining complex and chaotic structure-induced flow patterns. Xu et al. [57] studied a swirling flow combined with a vibrating wall in conical pipes by 2D PIV. Zhang et al. [58] used PIV, observing the turbulence performance of combining the honeycomb with the screens in a small open circulating flume. Under two filling rates and three baffle positions, Sterczyńska and Jakubowski [59] applied the PIV technique to monitor the cone-accumulating flow for a whirlpool tank in rotational motion. Based on previous work, the improvement of flow conditions in a whirlpool with a

modified bottom is further proposed by Sterczyńska et al. [60] using PIV measurements. In the research mentioned above, PIV is utilized to study the complicated flow structures by rigid structures with a range of hydraulic properties. As shown with these few examples, PIV is a great and universal tool with which to investigate turbulent flow.

The choice material and size of tracer particles are key components of PIV measurements. In this experiment, polyvinyl chloride (PVC-6500) micro-powders with a diameter of 50 μm, which have excellent flow-tracking and stable chemical properties, were used as the tracer particle. The high-resolution 2048 × 2048-pixel CCD (Charge Coupled Device) camera was used to continuously capture 300 instantaneous particle images at the frequency of 4.83Hz, which is the optimum value of the synchronization between camera and laser by a digital delay pulse generator. The test section was illuminated by a double pulsed Nd: YAG laser with a pulse intensity of 25mJ focused on a sheet of 2-m width. The model of the laser pulse synchronizer is 610036. The flow field measurement was performed with a horizontal region situated at 0.05 m above the flume bottom. The time-averaged flow fields over a 0.05-s interval were processed using the Insight 4G software PIV system. The PIV images were taken over an area of 380 mm (length) × 370 mm (width), which resulted in 3969 vectors (63 × 63) over the measured area. The measurement uncertainty was less than 0.005 pixels based on the particle diameter and particle density.

3. Results

3.1. Horizontal Flow Patterns

3.1.1. Flow Fields of a Single Groin and Symmetrical Groins

Time-averaged horizontal flow fields of a single and two symmetrical groins on the same horizontal plane (z/H = 0.05 m, where z is the height of velocity profile captured and H is the experimental water depth) are shown in Figure 4. In the flow field of a single groin, nearly stagnant flow with the lowest velocity appeared in the lee of Groin A due to the blockage effect of the groin and strong backflow was generated downstream from the stagnant flow, which eventually caused a large-scale recirculation zone. The downstream recirculation zone formed behind a groin was subdivided into three main zones, i.e., shear layer, backflow, and reattachment zone. Velocity differences are evident between the mainstream and the backflow behind Groin A; therefore, the original smooth flow pattern became chaotic due to the strong shear stress within the mixing layer at the interface of the mainstream and backflow. Figure 4a also shows the time-averaged reattachment point, where the separated flow reattaches to the flume wall on the right side of the groin, and the velocity vector is as often in the upstream direction (recirculation) as in the downstream direction (main flow). The time-averaged velocity of the reattachment point is approximately zero. The streamline from the groin tip to the reattachment point forms a recirculation zone containing a large-scale inner vortex, as depicted in Figure 5. In this study, the distance from the reattachment point to the groin wall (the side of facing downstream) is defined as the length of the recirculation zone formed behind the groin, i.e., backflow length; the maximum width of the recirculation zone is the backflow width. The observed backflow length was over five times the length of a single groin. On one hand, the mainstream velocity significantly increases from the groin tip to the opposite bank due to the decreased cross-section caused by protrusion of the groin, with a velocity gradient rapidly increasing near the groin tip, resulting in the shear layer zone (0.089 m/s $\geq v_{xy} \geq$ 0.030 m/s). On the other hand, the velocity behind the groin rapidly decayed, resulting in a low-velocity recirculation zone.

Figure 4b shows the horizontal flow field of two symmetrical single groins installed in both banks. Because the cross-section of main flow was further contracted by two groins, the velocity of the main flow increased more than that of a single groin. Another large-scale recirculation zone was formed behind Groin B. Due to the symmetrical arrangement of two identical groins, the two recirculation zones behind the groins were also symmetrically distributed, with identical inner vortical structures rotating in the opposite direction. The cross-section of main stream is narrowed down and the velocity profile from the groin tip

is reshaped by two recirculation zones, which would have significant effects on scouring in the main channel of a real-world river. The result is consistent with the study of Cuong et al. [42], which simply examined the impacts of groin length on flow fields around groin groups in a symmetrical configuration using Flow-3D software.

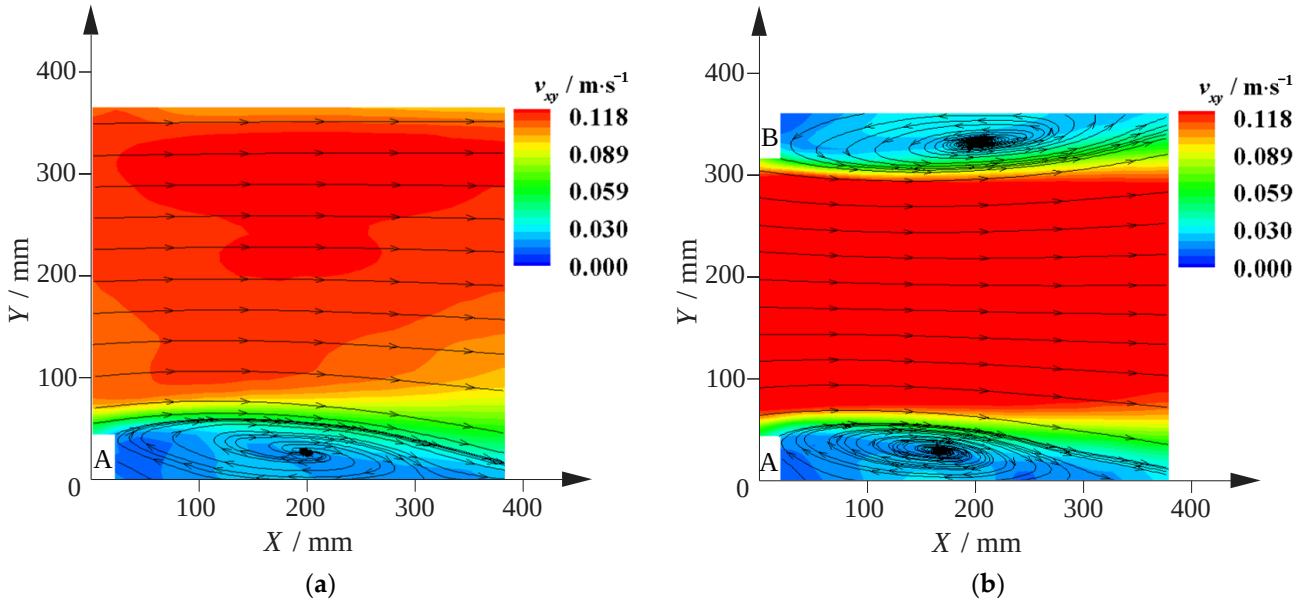

Figure 4. Time-averaged velocity distribution and streamlines of (**a**) a single Groin A and (**b**) two symmetrical Groins A and B: the color indicates the velocity magnitude.

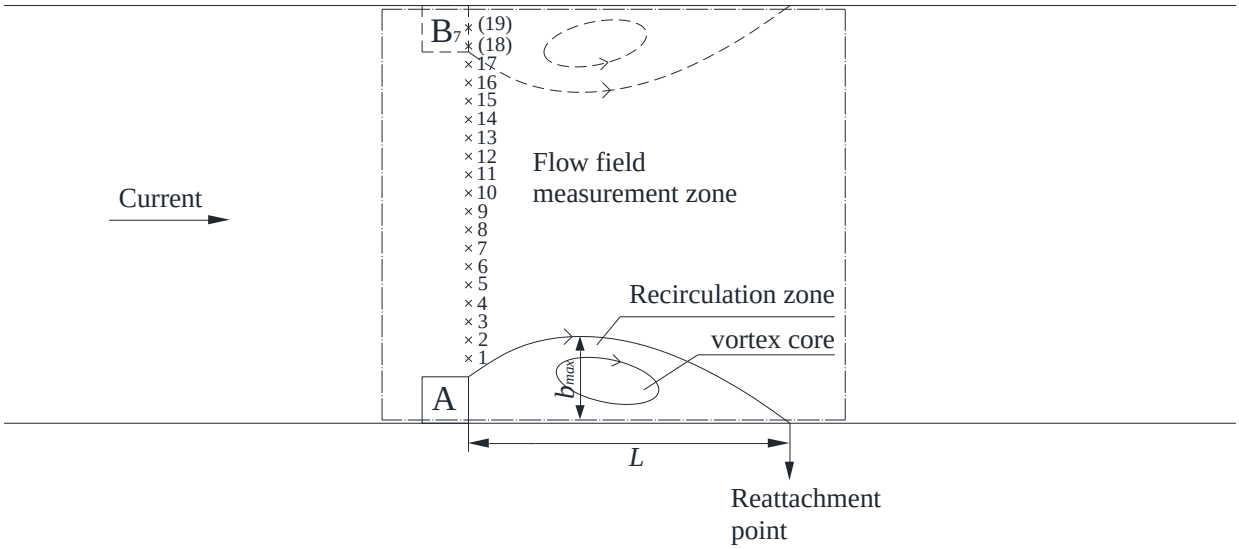

Figure 5. Schematic diagram of streamlines and observed points of velocities on the cross-section through the groin tip for the single groin (solid line) and symmetrical groins (dotted line), in which b_{max} indicates the backflow width and L represents backflow length (top view).

3.1.2. Flow Fields of Two Alternating Groins with Various Spacing

Figure 6 shows the time-averaged horizontal streamlines behind Groin A that are affected by Groin B located at the opposite bank with 5-, 15-, 25-, 35-, 45-, and 55-cm spacings upstream and downstream from Groin A. When Groin B is upstream from Groin A, the flow reattachment point of Groin A moves further downstream with increasing

spacing between groins, as shown in the left column of Figure 6. Likewise, the flow fields near Groin A with Groin B downstream, shown in the right column of Figure 6, indicate that the recirculation zone behind Groin A is significantly smaller than that with Groin B upstream. As a consequence, a smaller low-velocity zone was formed behind Groin A.

To quantify the evolution of backflow patterns behind Groin A with different spacings between the two groins, the main characteristic parameters of the recirculation zone behind Groin A are calculated and are listed in Table 1 for all test cases. The length and width of the recirculation zone are normalized by groin length b, as L/b and B/b, respectively. The width of the recirculation zone was expected to increase with increasing recirculation length. In the case of Groin B upstream from Groin A, the recirculation zone behind Groin A becomes larger than that without Groin B (namely Case 14, a single groin). The longest recirculation zone behind Groin A occurred during Case 5, where Groin B was located 0.15 m upstream from Groin A; the backflow streamwise length was over 50% more than that behind the single groin during Case 14. In contrast, when Groin B was deployed downstream from Groin A, the backflow size behind Groin A was smaller than that of a single groin. The recirculation zone behind Groin A reached a minimum when Groin B was 0.15 m downstream from Groin A (Case 9), where the recirculation length was more than 30% less than that behind a single groin. These results indicate that an upstream alternating Groin B promotes the development of a recirculation zone behind Groin A, whereas a downstream alternating Groin B inhibits the generation and propagation of reversing flow induced by Groin A.

The normalized length and width of the recirculation zone behind Groin A are shown in Figure 7. The variation of recirculation zone length can be divided into three subzones. First, Cases 1–5 are classified as upstream far-field. As Groin B moves toward Groin A, the main channel becomes narrower; therefore, the velocity is larger and the low-velocity zone at Groin B is expanded. The recirculation zone behind Groin A is lengthened from 0.314 to 0.384 m, about 20%. Second, Cases 6–8 are classified as the upstream and downstream near-field and symmetrical layout. The width of the channel between the groins was narrowed remarkably in these three cases, and the low-velocity zone near the groins reached the maximum for the symmetrical groin layout. The main channel was separated by groin tips and the fluid stream spread rapidly after bypassing Groin B due to fluid inertia, which significantly inhibited the backflow induced by Groin A. As a result, the recirculation zone behind Groin A was shortened from 0.35 to 0.17 m, about 50%. Third, Cases 10–13 are categorized as the downstream far-fields. As Groin B moves downstream far away from Groin A, the main channel next to Groin A was narrowed less and the low-velocity area at the opposite bank also became smaller than the other two subzones. Thus, the upstream fluid was mainly affected by the incoming flow. In this subzone, the length of the recirculation zone gradually increases again from 0.187 to 0.236 m, about 20%, which was similar to that for cases 1–5. In downstream far-field cases, the flow reattachment point behind Groin A moves further downstream with increasing spacing between groins, except for case 13, which was almost same as that of case 7, case 14 and the experimental results observed by Gu and Ikeda [39].

Two fitted curves of recirculation zone length for cases 1–5 and 9–13 in Figure 8 were presented for the relationship between the spacing of alternating groins and recirculation behind groin A with a correlation coefficient R^2 over 0.96. The result also suggests that as Groin B moves upstream and downstream from Groin A, the magnitude of impact Groin B has is similar to that on the wake flow behind Groin A; however, the flow direction is opposite.

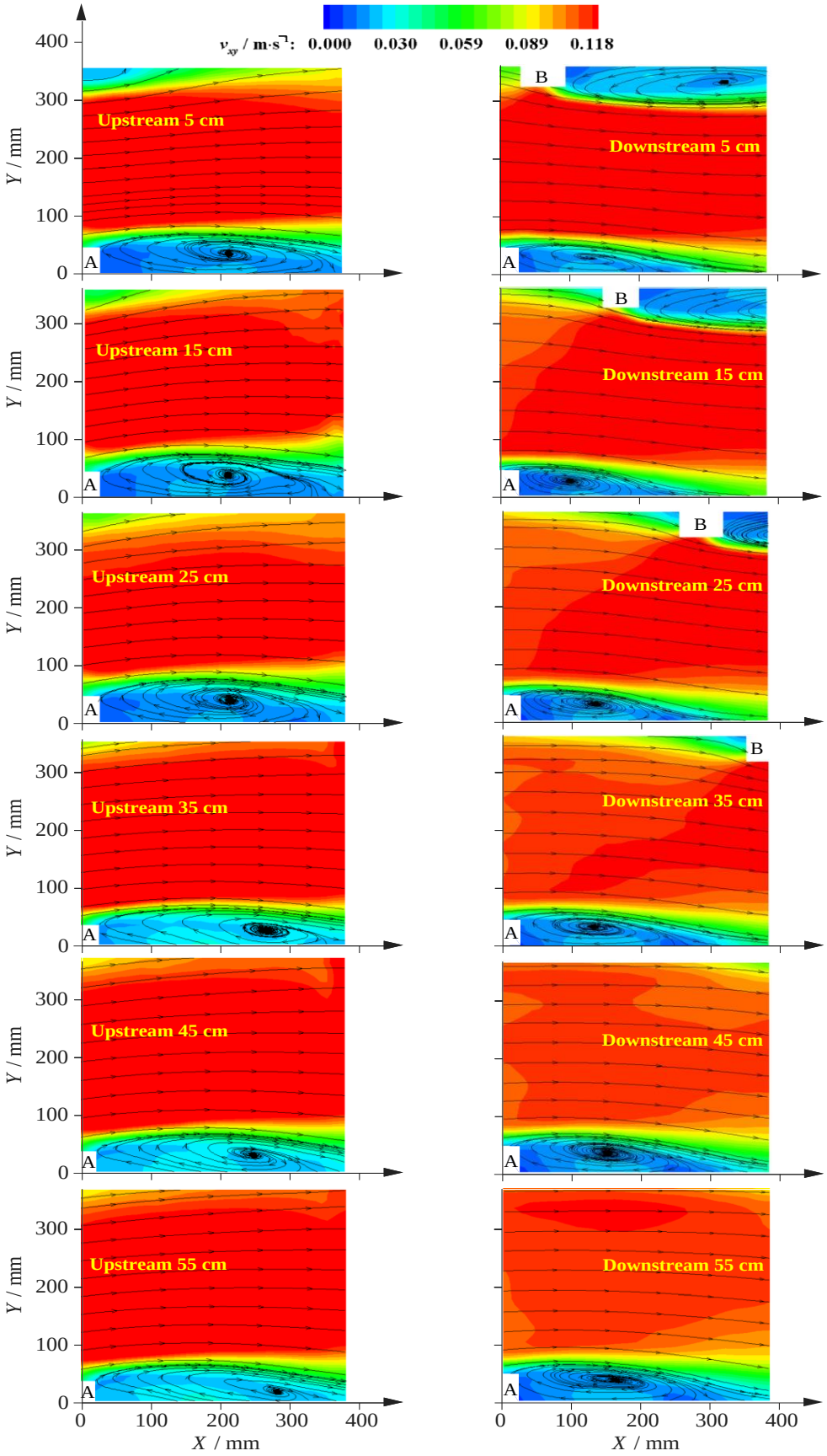

Figure 6. Time-averaged horizontal streamlines and velocity distribution of alternate groins configuration with Groin B at the opposite bank at 5 to 55 cm upstream (left column) and downstream (right column) from Groin A.

Table 1. Experimental results of the horizontal recirculation zone behind Groin A for different cases.

Case	Spacing between Groins/x (m)	Recirculation Zone Behind the Fixed Groin A				Feature
		Length/L (m)	Width/W (m)	Normalized Length (L/b)	Normalized Width (W/b)	
1	−0.55	0.314	0.073	6.276	1.465	Groin B moving upstream (alternate layout)
2	−0.45	0.325	0.077	6.506	1.534	
3	−0.35	0.345	0.078	6.903	1.552	
4	−0.25	0.355	0.081	7.063	1.616	
5	−0.15	0.384	0.082	7.683	1.630	
6	−0.05	0.350	0.075	6.999	1.504	
7	0.00	0.245	0.063	4.905	1.265	Symmetrical groins (both banks)
8	0.05	0.170	0.056	3.395	1.121	Groin B moving downstream (alternate layout)
9	0.15	0.160	0.057	3.193	1.149	
10	0.25	0.187	0.060	3.745	1.194	
11	0.35	0.212	0.064	4.234	1.276	
12	0.45	0.226	0.067	4.526	1.344	
13	0.55	0.236	0.067	4.721	1.334	
14	— —	0.250	0.066	5.002	1.329	Single Groin A

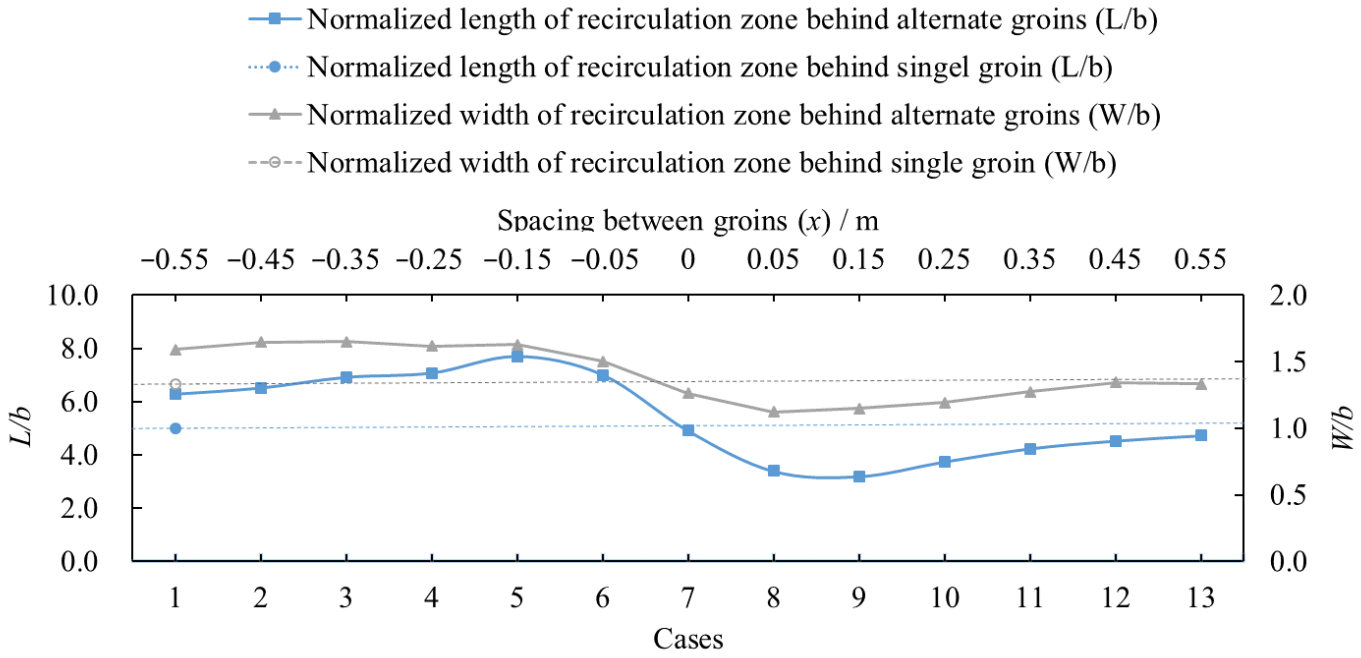

Figure 7. Normalized length L/b (left y-axis) and width W/b (right y-axis) of the recirculation zone behind a fixed Groin A as a function of the spacing (Top x-axis) between alternate groins on either side of river bank. The blue and gray circles are the normalized length of the recirculation zone for a single groin.

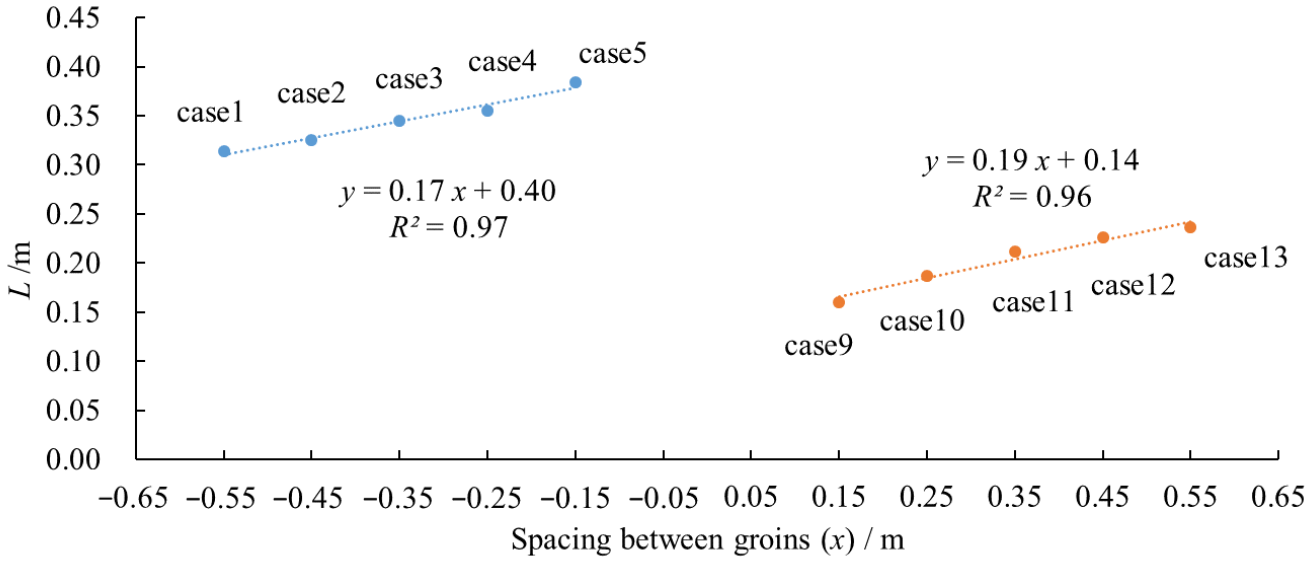

Figure 8. Relationship between the recirculation length behind Groin A (L) and the spacing between groins (x) for cases 1–5 and cases 9–13, respectively.

3.2. Velocity along Cross-Section through Groin Tip and Its Influence on Recirculation Zone

The flow field near a groin has a dominant effect on the backflow pattern behind the groin. Because the velocity near the groin tip is directly associated with the downstream turbulent intensity and the streamwise propagation of recirculating flow. Therefore, the time-averaged streamwise and spanwise velocity components at 19 points evenly distributed along the cross-section of the groin tip were extracted to examine their influence on the downstream recirculation. The schematic of observed points at the cross-section of a single groin is plotted in Figure 5; the positions of velocity observation points in the other cases of alternating groins are the same, except with only 17 points extracted for the symmetrical groins.

Figure 9 shows the time-averaged streamwise velocity component (i.e., x-velocity, v_x) of each observed point on the cross-section of Groin A. The streamwise velocity at points 1–3 nearest the groin tip and points 16–19 nearest the opposite bank varied markedly; however, at points 4–15 in the middle of the main channel it was hardly changed. The streamwise velocity reached the maximum near the fourth point in front of the groin, except for Case 7 (symmetrical groins), where the maximum velocity appears at the fifteenth point due to the other groin symmetrically deployed at the opposite bank, see Figure 9b. Overall, the variation time-averaged streamwise velocities at points 1–3 were similar to each other, i.e., the velocity linearly increased from point 1 to 3 due to the strong shear stress near the groin wall. However, the streamwise velocity at points 16–19 decreased and the variation of each case varied notably, which implies that streamwise velocity at the opposite bank is not simply affected by the contacted section of groin but also by the flume wall. The streamwise velocity represents the water flux through the cross-section of the main channel, and plays a leading role on the flow structure near Groin A and further alters the backflow induced by the groin.

The averaged streamwise velocity of points 16–19 (denoted as $\overline{v_{x,16-19}}$) for each case and the length of the recirculation zone are correspondingly presented in Figure 10, in which the negative value of spacing between groins represents Groin B located upstream of Groin A. It is obvious that $\overline{v_{x,16-19}}$ had completely different properties with various locations of Groin B. When Groin B was located in the upstream far-field and moves towards Groin A (Cases 1–5), with shorter spacing between groins, the streamwise velocity gradually decreased because the upstream cross-section of Groin A contracted continuously, so that the length of the recirculation zone behind Groin A progressively increased. In particular,

the minimum of $\overline{v_{x,16-19}}$ and the maximum of backflow length appeared in Case 5, in which the spacing between groins was 0.15 m. When Groin B was deployed in the near-field (Cases 6–8) since groins too close to one another will prevent flow reattachment, keeping the shear stress between groins rather low, the change of streamwise velocity varied and the backflow length rapidly decreased the in above three cases. As Groin B was placed in the downstream far-field (Cases 9–13), $\overline{v_{x,16-19}}$ and recirculation length gently increased again because the narrowed cross-section was gradually wider with Groin B away from Groin A.

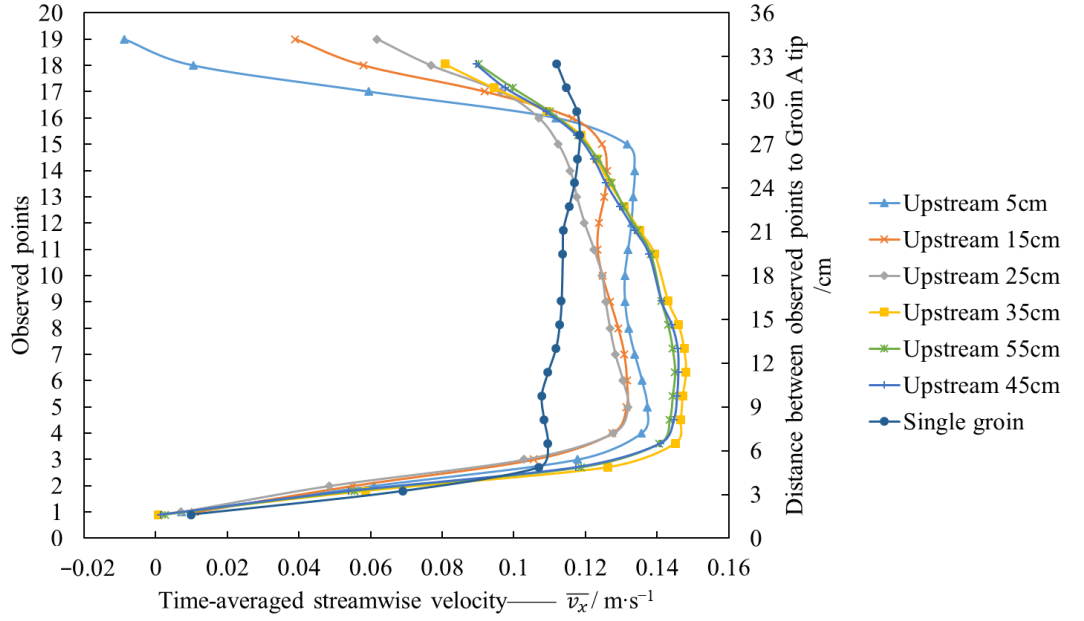

(**a**)

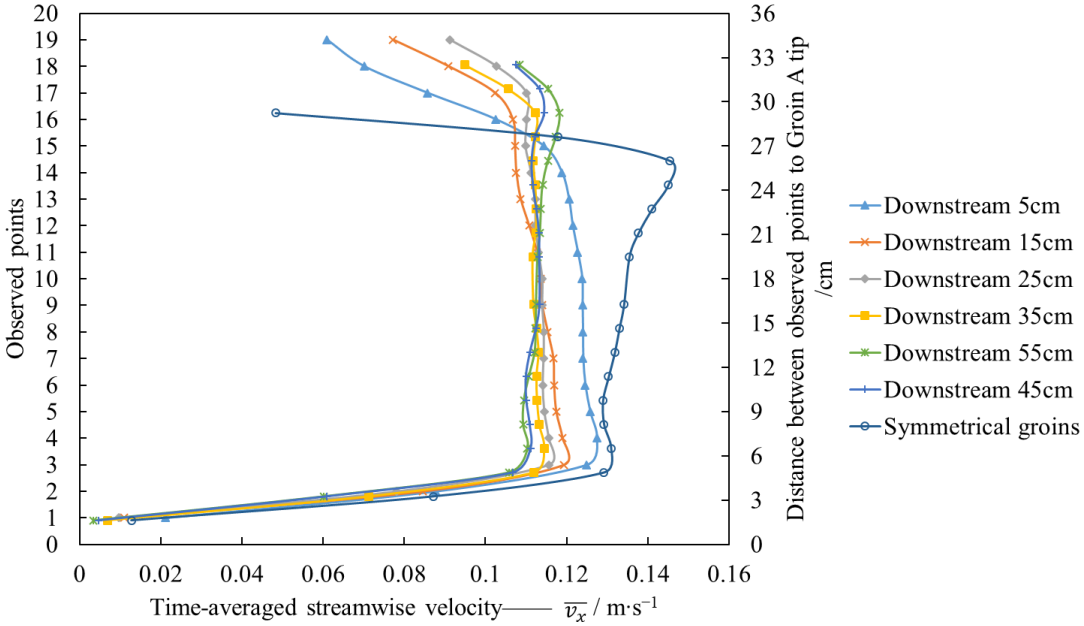

(**b**)

Figure 9. Time-averaged streamwise velocity ($\overline{v_x}$) at the observed points along the cross-section located at Groin A tip for (**a**) single groin and Groin B located at upstream of Groin A; (**b**) symmetrical groins and Groin B located downstream of Groin A.

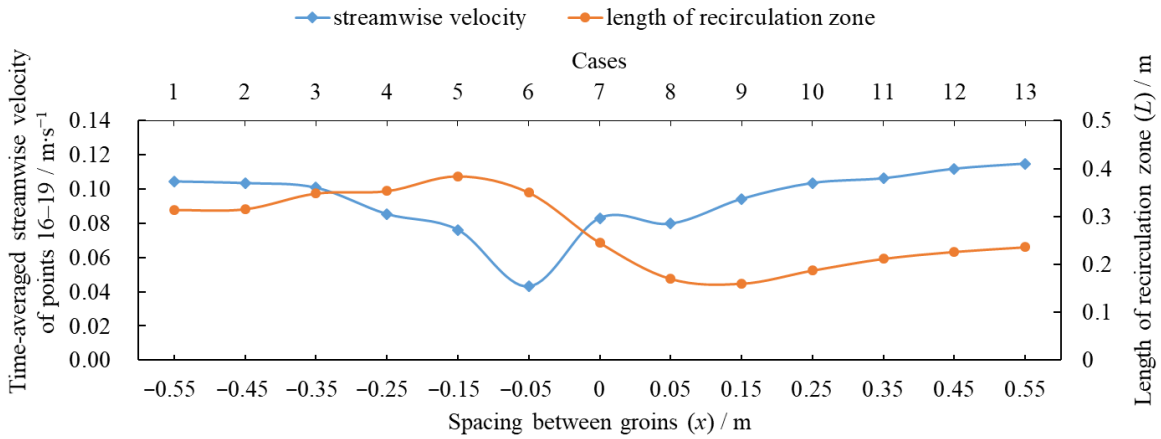

Figure 10. Time-averaged streamwise velocity at observed points (16~19) along the cross-section located at the Groin A tip and the length of the recirculation zone behind Groin A for each case.

Figure 11 shows the relationship between time-averaged spanwise velocity (i.e., y-velocity, $\overline{v_y}$) at points 1–3, 4–15 and 16–19 along the cross-section of Groin A and the width of recirculation zone. It was found that the time-averaged spanwise velocity on the cross-section through Groin A tip relates approximately linearly to the recirculation zone width. The linear relationship between $\overline{v_y}$ at points 1–3 and recirculation zone width has a coefficient of determination R^2 of 0.96. The R^2 between the recirculation zone width and $\overline{v_y}$ at points 4–15 reaches 0.95. The velocity distributed on the fitted line of points 1–3 were closer to each other than that of other points. In other words, the linear relationship works the best between $\overline{v_y}$ at points 1–3 and the width of recirculation zone, which implies that correctly representing the spanwise velocity nearest the groin tip is the most important factor in determining the recirculation zone width.

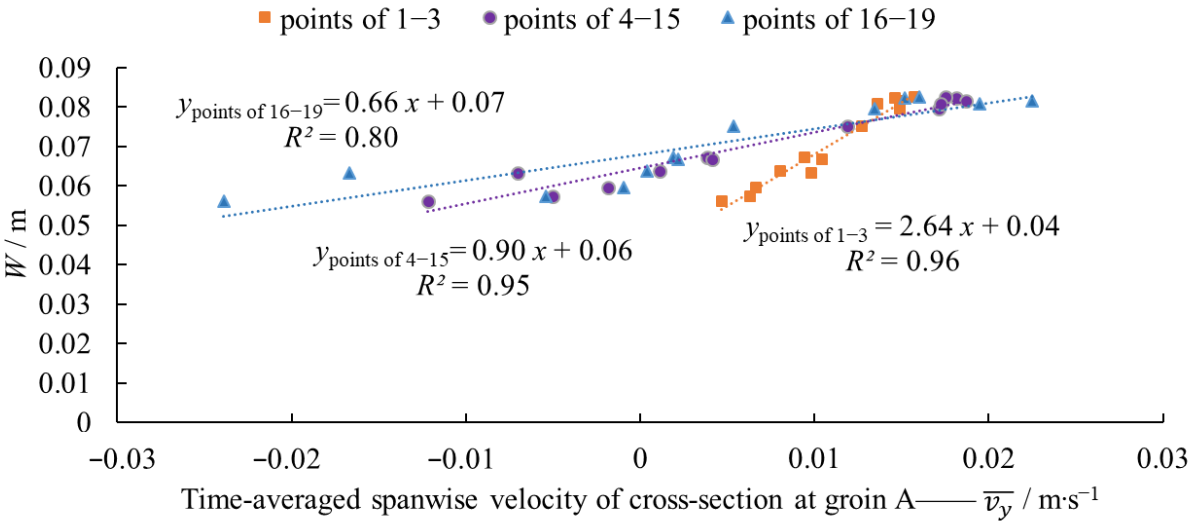

Figure 11. Relationship between the time-averaged spanwise velocity ($\overline{v_y}$) of observed points along the cross-section through Groin A and the width of the recirculation zone (W) behind Groin A.

The relationship between the width and length of the recirculation zone formed behind Groin A is shown in Figure 12, with the fitting accuracy R^2 of 0.96. It is known that the spanwise velocity at points 1–3 nearest the groin tip has a significant effect on the width of the recirculation zone (see Figure 11), which in turn affects the length of the recirculation zone (see Figure 12). In other words, the influence of Groin B on the flow structure around

Groin A is mainly manifested in the degree of river reach shrinkage and spanwise velocity change near the tip of Groin A.

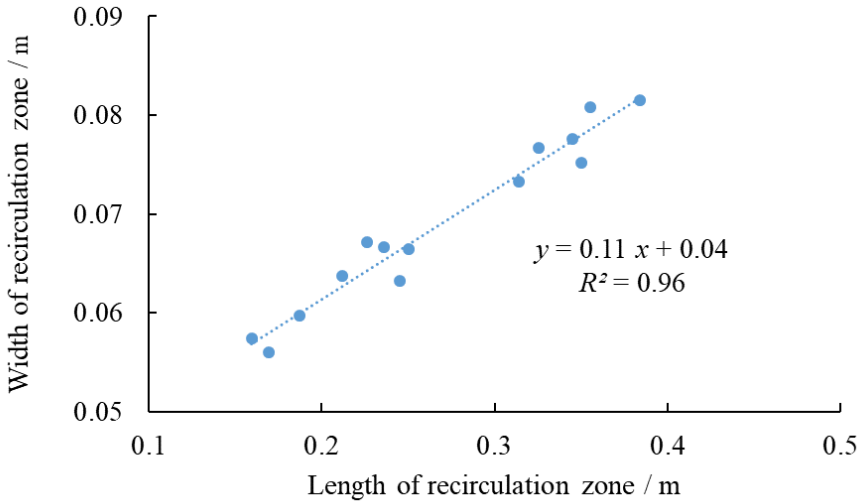

Figure 12. Relationship between the length and width of the recirculation zone behind Groin A.

3.3. Vorticity Distribution and Its Influence on Recirculating Flow

Based on the measured data, the vertical vorticity (i.e., z-component of vorticity, Ω_z) component is calculated using the following equation,

$$\Omega_z = \frac{\partial v_y}{\partial x} - \frac{\partial v_x}{\partial y} \quad (1)$$

where v_x is the velocity in the streamwise, x-direction; v_y is the velocity in the spanwise, y-direction; and Ω_z is vertical rotational strength of the recirculating flow. The vorticity distribution plays a leading role in the research of recirculating flow, particularly the flow behind some rigid structures such as groins [36].

Figure 13 shows the vertical vorticity (magnitude indicated by colors) distributed in the horizontal measured plane for one single groin and two symmetrical groins. The maximum vertical vorticity occurred near the groin tip, as illustrated in Figure 13a. The observed vertical vorticity pattern of a single groin is consistent with the previous numerical results from Duan [15]. The vertical vorticity Ω_z generated by a single groin is manifested as the negative vertical vorticity Ω_z downstream, which originates from the groin tip and is concentrated within the mixing layer zone. Interestingly, as Groin B was symmetrically placed at the opposite bank to Groin A, the maximum positive vertical vorticity was induced by Groin B, where flow in the vicinity of the Groin A tip was dominated by high negative vertical vorticity along the recirculation zone, see Figure 13b. Since the propagation of negative vertical vorticity induced by Groin A was blocked at the transverse direction, two high-vorticity zones with similar size but opposite orientation symmetrically showed along the mixing layer zone behind Groins A and B. The velocity gradient in the mixing layer greatly increased due to the contraction of main flow by two symmetrical groins; as a result, the high-vorticity zones at both banks were extended further longitudinally compared to that of a single groin.

Figure 14 shows the vertical vorticity distribution of two alternating groins with various spacing between groins, downstream from Groin A. The vorticity fields also display distributions similar to the recirculation zone behind Groin A shown in Figure 5 for different test cases. High vorticity appeared at the mixing layer at the interface between the mainstream and recirculation zones. When Groin B was upstream of Groin A, the extent of high-vorticity was larger compared to that of Groin B downstream of Groin A. In addition, when Groin B was downstream of Groin A, the advection and diffusion of vorticity induced

by Groin A was hindered by the three-dimensional flow patterns over Groin B. Therefore, a smaller high-vorticity zone was formed behind Groin A and it skewed more to the flume wall, which impeded the formation of large-scale recirculation downstream of Groin A.

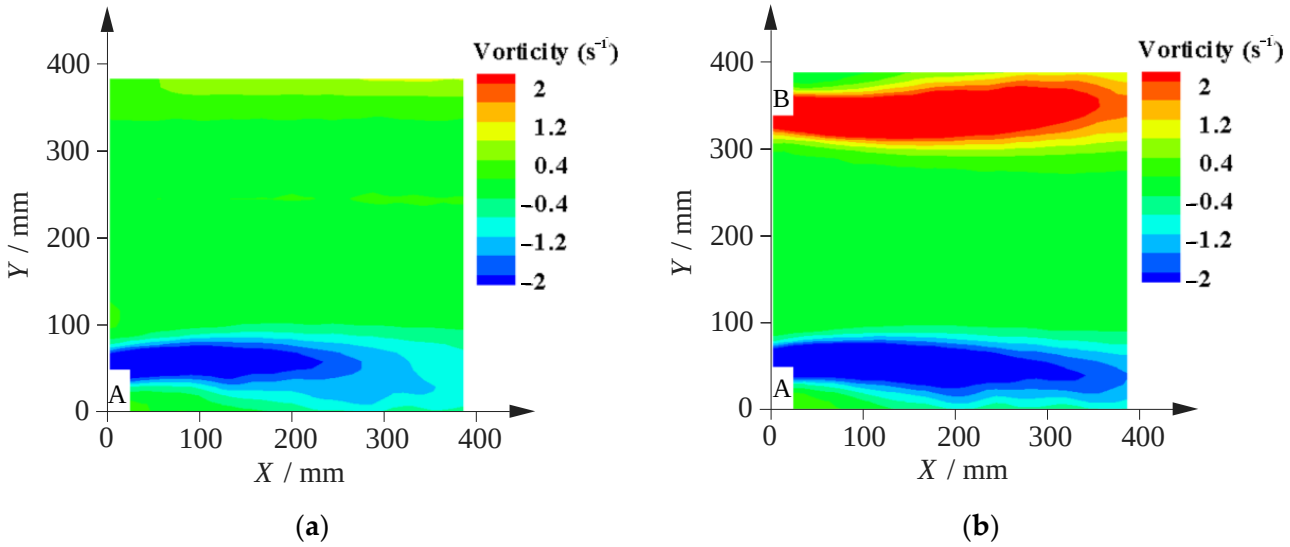

Figure 13. Vertical vorticity in the horizontal plane for (**a**) single groin, (**b**) two symmetrical groins.

Furthermore, the vertical vorticity flux (E_z) is introduced to describe the spatially integrated scalar value of Ω_z and the bulk effect of vertical vorticity on the downstream recirculation zone, defined as:

$$E_z = \iint \Omega_z dxdy = \iint \left(\frac{\partial v_y}{\partial x} - \frac{\partial v_x}{\partial y}\right) dxdy \quad (2)$$

where the integration area is the whole horizontal plane measured by the PIV system.

The vertical vorticity flux through the whole horizontal plane measured by the PIV is calculated from Equation (2) and plotted in Figure 15, which also shows the recirculation zone length for different cases. The vertical vorticity flux E_z vs. recirculation zone length displays a consistent variation trend for different test cases. The vertical vorticity flux E_z increases with increasing recirculation zone length, resulting in more dissipation of flow energy. The variation of E_z vs. recirculation zone length displays three distinct subzones' response to the position of Groin B relative to Groin A, i.e., increase in the upstream far-field, decrease in the near field, followed by increase in the downstream far-field. The relationship between vertical vorticity flux and recirculation zone length in each subzone is shown in Figure 16. When Groin B is located upstream far-field of Groin A, the recirculation zone length behind Groin A increases at the fastest rate with increasing vertical vorticity flux. When Groin B is in the downstream far-field of Groin A, the recirculation zone length behind Groin A increases at the slowest rate with increasing vertical vorticity flux. The change rate of recirculation zone length is between the two above if Groin B is placed in the up- or down-stream near-field of Groin A. In summary, the accumulation effect of the vertical vorticity flux near Groin A is at its maximum when Groin B is located in the upstream far-field from Groin A.

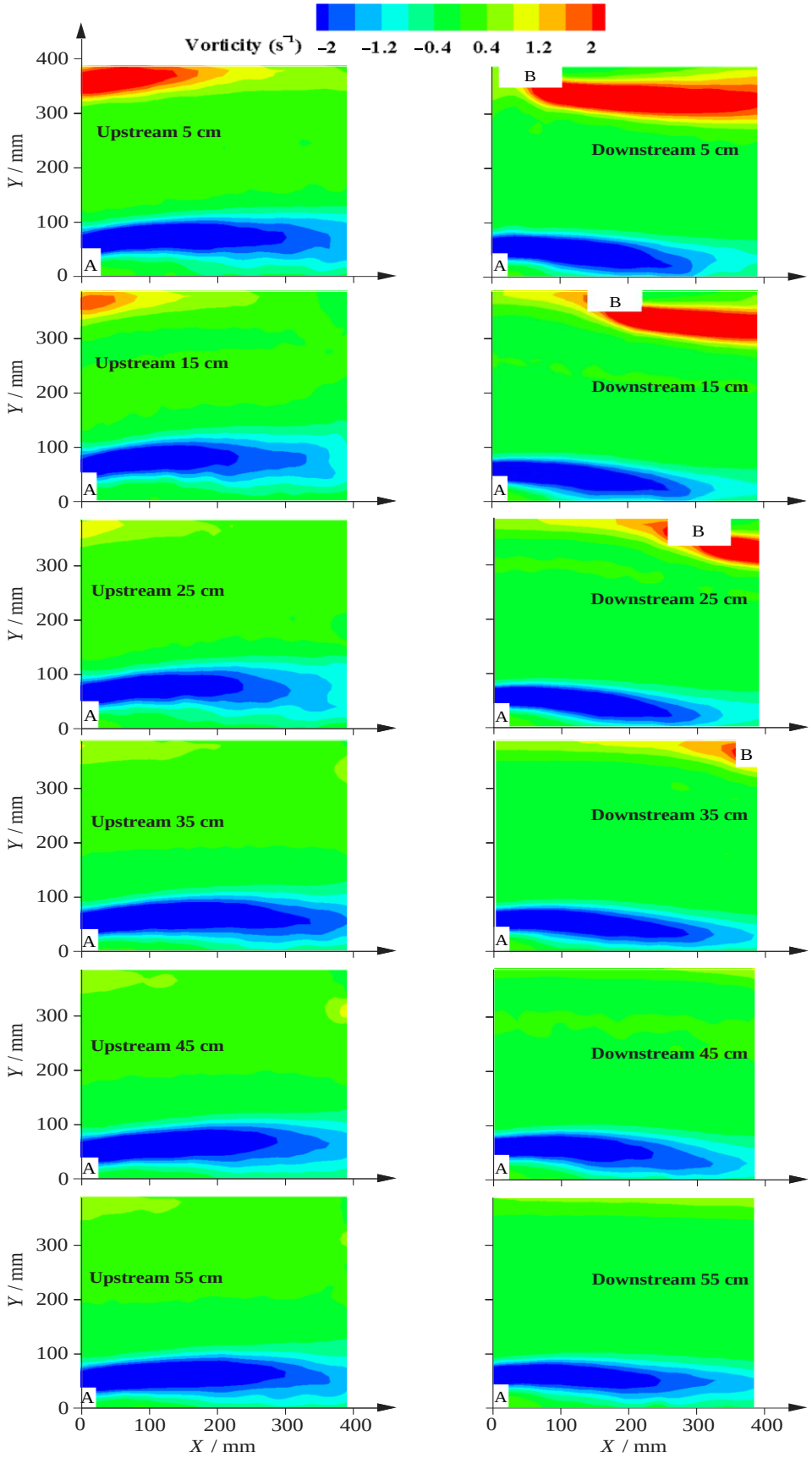

Figure 14. Vertical vorticity in the horizontal planes for alternating groin configuration with Groin B at 5 to 55 cm upstream (left column) and downstream (right column) from Groin A.

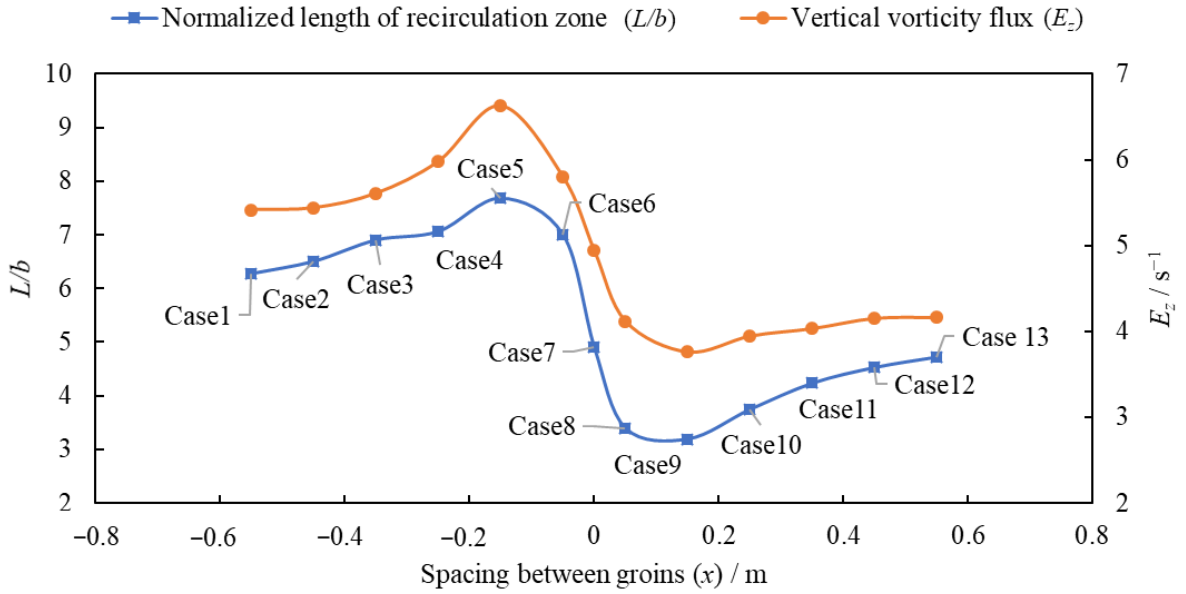

Figure 15. Variation of recirculation zone length behind Groin A with the vertical vorticity flux induced by Groin A for different spacing between groins.

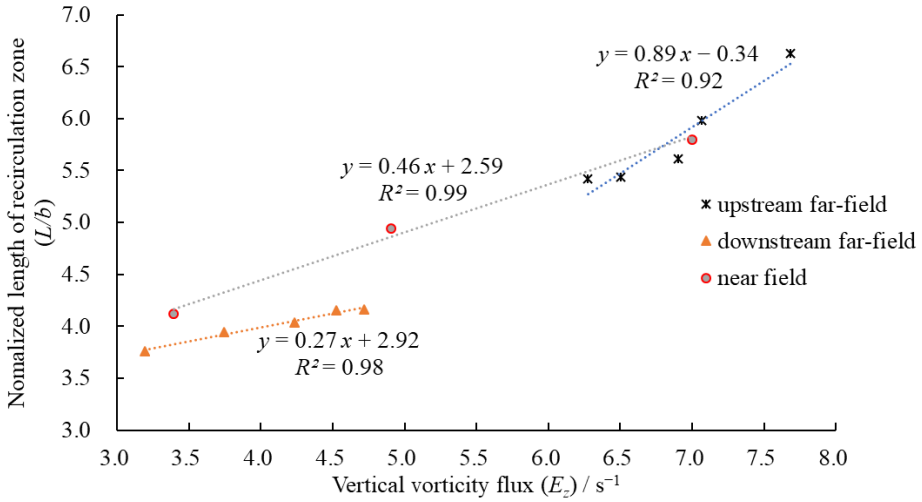

Figure 16. The relationship between vertical vorticity flux and recirculation zone length of Groin A when Groin B is upstream far-field (black *), downstream far-field (orange triangle) and near field (red circle) from Groin A.

As Groin B approaches Groin A on the upstream side, the advection and diffusion of vorticity induced by Groin A in the horizontal plane are enhanced and the extent of high vertical vorticity flux area increases, resulting in a larger recirculation zone. In case 7, i.e., symmetrical groins, a critical threshold appears in the extension of vertical vorticity flux produced by Groin A both in transverse and longitudinal directions, which demonstrates that the transverse extension of vertical vorticity is strengthened whereas the longitudinal propagation of vertical vorticity is weakened significantly. It follows that the high-vorticity zone shrank, leading to a shorter recirculation zone behind Groin A. When Groin B is 0.15 m downstream of Groin A, the streamwise extension of the vertical vorticity induced by Groin A is inhibited the most by Groin B so that the length of the recirculation zone behind Groin A drops to the minimum value of 0.16 m (see Table 1). When the groins are

further apart, downstream Groin B promotes the increase in vertical vorticity near Groin A, therefore promoting the development of the recirculation zone behind groin A. Although the vertical vorticity induced by Groin A is a nonlinear function of the Groin B distance from Groin A, the variation rate of vertical vorticity flux and the recirculation zone length induced by Groin A remains almost constant.

4. Discussion

4.1. Effect of Backflow Patterns of Groin B on Recirculation Zone Behind Groin A

The flow interaction between bilateral groins determines the contraction extent of the main channel by groins with different spacing, which further influences the downstream backflow affected by the streamline curvature. It implies that the deformation of streamlines passing groins is important to the development of the recirculation zone behind Groin A. When Groin B is placed upstream of Groin A, the outward normal direction of flow at the end of the recirculation zone induced by Groin B points toward Groin A and the convex recirculation zone behind Groin A concurrently (see Figure 17a). It can be interpreted as the flow pointing towards the rear of Groin B along the section in the outward normal direction, which provides additional momentum to downstream recirculating flow induced by Groin A, resulting in a larger velocity component pointing to the opposite river bank. With Groin B approaching Groin A, the width of the section along the outward normal direction decreases, but the current velocity on the section increases correspondingly to conserve mass, especially the velocity component in the transverse direction (i.e., spanwise velocity) because the angle between the outward normal direction and the flow direction become larger. As previously mentioned in Section 3.2, the spanwise velocity near the groin tip has a positive effect on the scale of the recirculation zone formed behind Groin A (see Figure 11), so that the laterally confined flow promotes the development of backflow behind Groin A. However, if Groin B is nearly symmetrical with Groin A on both banks, the outward normal direction of flow along the recirculation behind Groin B is no longer pointing to Groin A but to the downstream backflow of Groin A, as shown in Figure 17b. Eventually, the longitudinal propagation of the recirculation zone is limited, and the reattachment point moved towards Groin A.

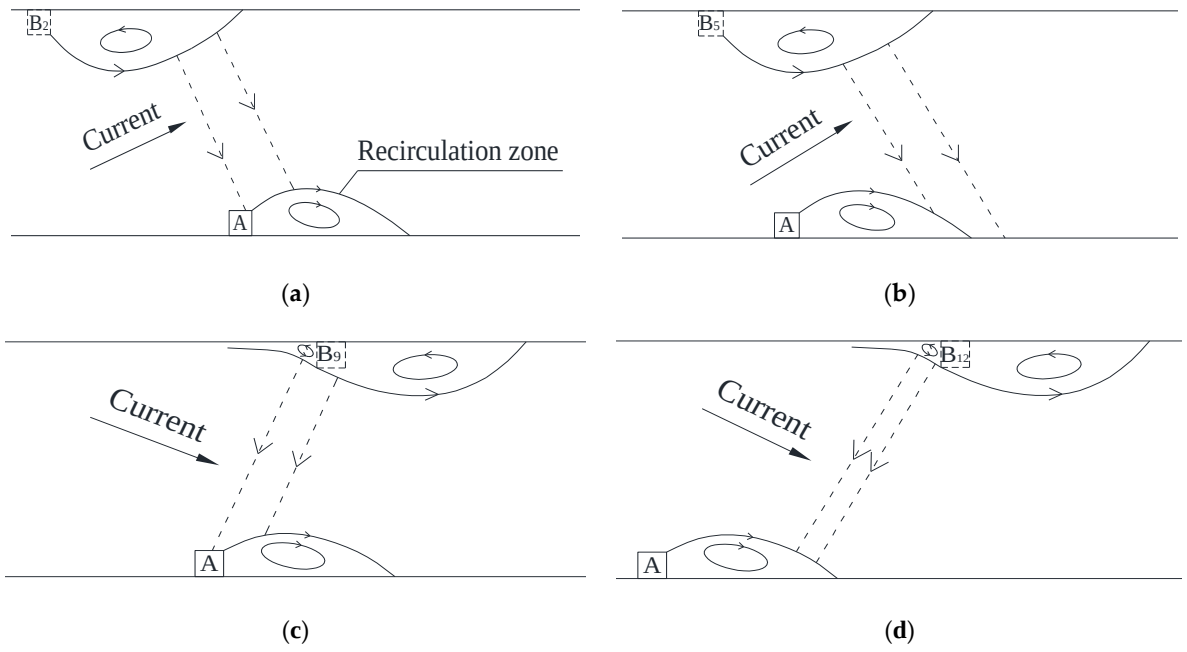

Figure 17. Schematic diagram of the influence of Groin B on the backflow behind Groin A in different cases, (**a**) Groin B in the upstream far-field of Groin A, (**b**) Groin B in the upstream near-field of Groin A, (**c**) Groin B in the downstream near-field of Groin A, (**d**) Groin B in the downstream far-field of Groin A.

Conversely, when Groin B is located in the downstream near-field of Groin A, the velocity distribution at the cross-section of Groin A would be shifted by the separating flow in front of Groin B, which is caused by the upstream corner vortex due to the blockage of Groin B. The outward normal direction of flow at the upstream part of the recirculation zone behind Groin B accordingly points to Groin A and the downstream recirculating flow induced by Groin A, see Figure 17c. With the joint actions of the flow at the front and rear of Groin B, more flow energy is dissipated near the tip of Groin A, where the maximum turbulent intensity appeared. Consequently, the spanwise velocity near the groin tip decreases further, and thus, the recirculation length of Groin A becomes smaller due to the dissipation of turbulent mixing energy. When groins are further apart (over 0.15 m), the angle between the downstream direction and current direction becomes smaller, leading to the angular momentum of mean flow increasing along the outward normal direction of recirculating flow induced by Groin B. Similar phenomena were observed by Gu and Ikeda [39] for groins in alternate layout. The front streamlines of separating flow induced by Groin B become gradually skewed and almost parallel to the rear streamlines of the recirculation zone behind Groin A. The outward normal direction of the front streamline along the recirculation zone of Groin B mainly points to backflow behind Groin A, resulting in more momentum concentrated in the recirculation zone (see Figure 17d). Thus, the spanwise velocity along the outward normal direction of streamline increases and transfers more kinetic energy to enhance the development of backflow behind Groin A.

4.2. Formula of Recirculation Zone Length Behind a Single Groin

Based on the energy equation, Dou et al. [61] considered the contraction ratio of the cross-section through a single groin and used the momentum conservation equation of separating flow. They proposed a hypothesis for the surface gradient of the mainstream and the turbulence shear stress of the boundary between mainstream and backflow. The formula for evaluating the recirculation zone length behind a single groin arranged perpendicular to the river bank was derived through integration of the governing equation, such that,

$$\ln \frac{B}{B-b_x} = -[A_1(1-\frac{x}{L})^2 + A_2(1-\frac{x}{L}) - \frac{L}{C_0^2 H}(1-\frac{x}{L}) - \frac{2A_3}{3}(1-\frac{3x}{2L}+\frac{x^3}{2L^3})\frac{L}{b_a} \quad (3)$$

where C_0 is the dimensionless Chezy formula and $C_0 = \frac{C}{\sqrt{g}}$; H is the water depth, which does not change much generally, and therefore the main water depth or the tailgate water depth is not affected by the groin and can be taken as constant; A_1, A_2 and A_3 are variable coefficients. The detailed definition of each parameter in Equation (3) is shown in Figure 18.

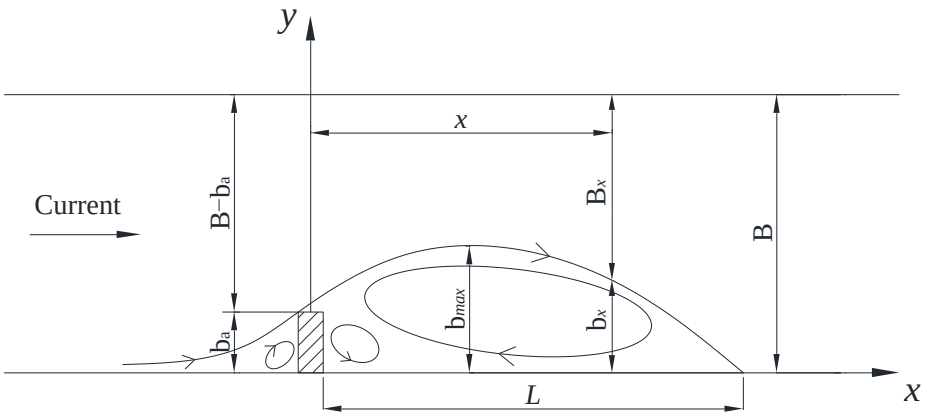

Figure 18. Schematic diagram of the recirculation zone behind a single groin.

Although the backflow pattern of Groin A is affected by Groin B on the opposite bank, the recirculation zone remained intact as a whole due to the thickness of short groins being

less than a third of the flume width. The scale of the downstream recirculation zone was influenced by both the constriction ratio of the cross-section through groins and spanwise velocity in front of the groin tip. According to the statistical results listed in Table 1, the length of recirculation zone for a single Groin A (Case 14), which is 0.25 m, is close to that of symmetrical groins (Case 7) and Groin B deployed 0.55 m downstream (Case 13). In addition, the averaged spanwise velocity of observed points distributed nearest to the groin tip are also similar to each other in the above three cases. Hence, based on the empirical formula regarding the recirculation length of a single groin [61], using the experimental data, a re-calibration was conducted for the relevant variables. The parametric relationship between two alternate groins and one single groin was established for the groin-induced recirculation zone.

In the parameter pre-calibration, three stochastic points on the boundary line of the recirculation zone behind a single groin were chosen, extracting x and y coordinates, respectively. The coordinates of each point were substituted into Equation (3), which established three equations correspondingly. A_1, A_2 and A_3 were determined by solving the equations. Meanwhile, one more point was extracted from the boundary line of the recirculation zone, and then the x coordinate of the point and solved parameters A_1, A_2 and A_3 were substituted into Equation (4). Accordingly, the basic formula of downstream recirculation length (L'_a) for a single groin was obtained as follows:

$$L'_a = \frac{C_0^2 H b_a}{0.223 C_0^2 H + b_a}\left(1 + \ln \frac{B}{B - b_a}\right) \tag{4}$$

4.3. Formula of Recirculation Zone Length Behind Alternating Groins

As previously analyzed in Section 3.1, there are three subzones for the variation of backflow length behind Groin A with the various spacing between groins, i.e., upstream far-field (Cases 1–5), near-field (Cases 6–8) and downstream far-field (Cases 9–13), as a result, the calculation of the backflow length behind Groin A can also be divided into three subzones.

When Groin B is on the opposite bank and upstream/downstream far-field of Groin A, the influence of Groin B on the backflow length behind Groin A can be represented by the relative contraction ratio of cross-section (δ_b), and given as:

$$\delta_b = \left(\frac{B}{|x| + B} b_b\right)/B \tag{5}$$

The total contraction ratio of the cross-section in front of Groin A due to Groins A and B (δ_{ab}) is given as:

$$\delta_{ab} = \left(b_a + \frac{B}{|x| + B} b_b\right)/B \tag{6}$$

Thus, the passing ratio of main flow through the cross-section is given as:

$$\delta = 1 - \delta_{ab} = 1 - \left(b_a + \frac{B}{|x| + B} b_b\right)/B \tag{7}$$

When Groin B is in the near-field of Groin A, the relative contraction ratio of Groin B to Groin A (δ_b) can be expressed as:

$$\delta_b = \left(\frac{B - x}{B} b_b\right)/B \tag{8}$$

The total contraction ratio of the cross-section in front of Groin A from Groins A and B (δ_{ab}) becomes:

$$\delta_{ab} = \left(b_a + \frac{B - x}{B} b_b\right)/B \tag{9}$$

The current crossing capacity of a river section (δ) becomes:

$$\delta = 1 - \delta_{ab} = 1 - (b_a + \frac{B - x}{B} b_b)/B \tag{10}$$

In Equations (5)–(10), B is river width, b_a and b_b are the lengths of Groins A and B, respectively, x is the longitudinal spacing between Groins B and A (the x value is negative and positive responding to the location of groin B upstream and downstream from Groin A, respectively). According to the variation process in Figure 6, a linear relationship between recirculation zone length and spacing of groins can be observed (see Figure 7), indicating that linearity exists with the contraction ratio of a cross-section through groins. The contraction ratio comprehensively reflects the influence of the opposite Groin B on the flow structure around the Groin A, especially the spanwise velocity in the vicinity and rear of Groin A. Hence, the relationship between the backflow length of Groin A under the impact of Groin B (L_a) and the backflow length of a single groin (L'_a) can be given as follows:

$$\frac{L_a}{L'_a} = f(\frac{\delta}{\delta'_a}) \tag{11}$$

where

$$\delta'_a = \frac{(B - b_a)}{B} \tag{12}$$

When Groin B is in the upstream far-field of Groin A, the relationship diagram of $L_a/L'_a \sim \delta/\delta'_a$ is drawn by experimental data; the result is shown in Figure 19.

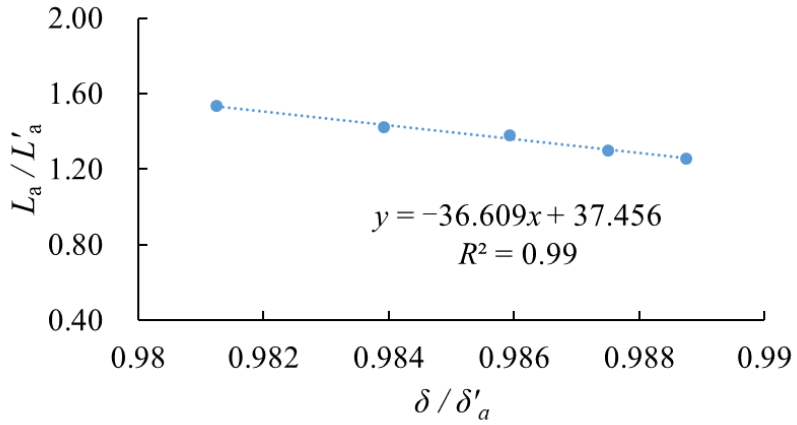

Figure 19. The relationship between L_a/L'_a and δ/δ'_a when groin B is in the upstream far-field of groin A.

According to the linear fitting formula in Figure 19, Equation (11) can be written as:

$$\frac{L_a}{L'_a} = -36.609(\frac{\delta}{\delta'_a}) + 37.456 \tag{13}$$

Furthermore, Equation (4) is substituted into Equation (13), and the length of recirculation zone behind Groin A can be obtained as:

$$L_a = \left[-36.609(\frac{\delta}{\delta'_a}) + 37.456\right] \frac{C_0^2 H b_a}{0.223 C_0^2 H + b_a} (1 + \ln \frac{B}{B - b_a}) \tag{14}$$

When Groin B is in the near-field of Groin A, the relationship diagram of $L_a/L'_a \sim \delta/\delta'_a$ is plotted in Figure 20.

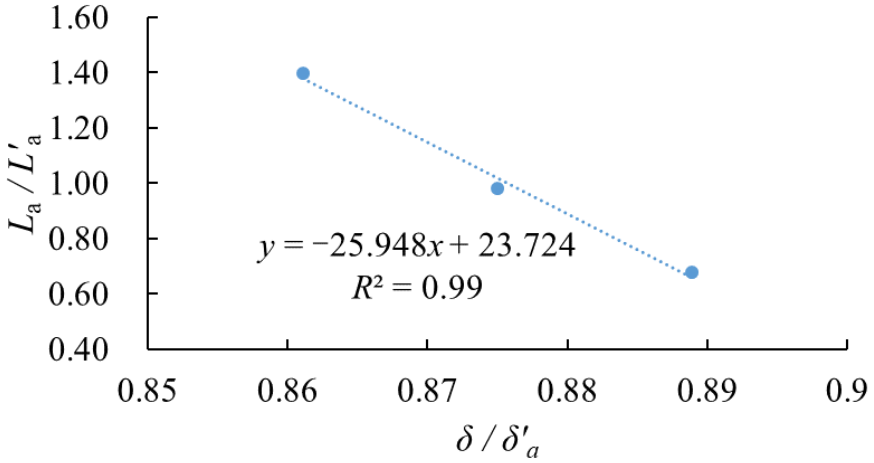

Figure 20. The relationship between L_a/L'_a and δ/δ'_a when groin B is in the near-field of groin A.

According to the linear fitting formula in Figure 20, Equation (11) can be written as:

$$\frac{L_a}{L'_a} = -25.948\left(\frac{\delta}{\delta'_a}\right) + 23.724 \tag{15}$$

Furthermore, Equation (4) is substituted into Equation (15), and the length of recirculation zone behind Groin A can be obtained as:

$$L_a = \left[-25.948\left(\frac{\delta}{\delta'_a}\right) + 23.724\right] \frac{C_0^2 H b_a}{0.223 C_0^2 H + b_a}\left(1 + \ln \frac{B}{B - b_a}\right) \tag{16}$$

When Groin B is at downstream far field of Groin A, the relationship diagram of $L_a/L'_a \sim \delta/\delta'_a$ is presented in Figure 21.

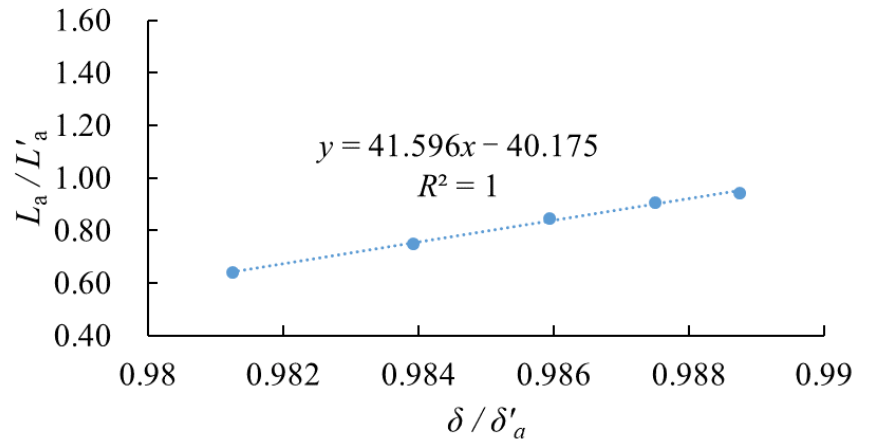

Figure 21. The relationship between L_a/L'_a and δ/δ'_a when groin B is in the downstream far-field of groin A.

Based on the linear fitting formula in Figure 21, Equation (11) can be written as:

$$\frac{L_a}{L'_a} = 41.596\left(\frac{\delta}{\delta'_a}\right) - 40.175 \tag{17}$$

Furthermore, substituting Equation (4) into Equation (17), the corresponding length of the recirculation zone behind Groin A can be obtained as follows:

$$L_a = \left[41.596\left(\frac{\delta}{\delta'_a}\right) - 40.175\right] \frac{C_0^2 H b_a}{0.223 C_0^2 H + b_a}\left(1 + \ln \frac{B}{B - b_a}\right) \tag{18}$$

Consequently, when groins were arranged in an alternating layout on both river-banks, the length of the recirculation zone behind the single groin affected by another groin on the opposite bank can be assessed using the following equations for various longitudinal spacing between groins (x):

$$L_a = \begin{cases} \left[-36.609\left(\frac{\delta}{\delta'_a}\right) + 37.456\right] \frac{C_0^2 H b_a}{0.223 C_0^2 H + b_a}\left(1 + \ln \frac{B}{B - b_a}\right), \ (x \leq -0.15 \text{ m}) \\ \left[-25.948\left(\frac{\delta}{\delta'_a}\right) + 23.724\right] \frac{C_0^2 H b_a}{0.223 C_0^2 H + b_a}\left(1 + \ln \frac{B}{B - b_a}\right), \ (-0.15 \text{ m} < x < 0.15 \text{ m}) \\ \left[41.596\left(\frac{\delta}{\delta'_a}\right) - 40.175\right] \frac{C_0^2 H b_a}{0.223 C_0^2 H + b_a}\left(1 + \ln \frac{B}{B - b_a}\right), \ (x \geq 0.15 \text{ m}) \end{cases} \tag{19}$$

5. Conclusions

This study experimentally investigated the backflow patterns around a groin pair deployed at both banks with different spacing using PIV measurements and compared with the backflow pattern of a single groin.

For the short groin models used in the present experiment, the length and width of the recirculation zone behind a single groin are approximately 5 and 1.3 times the groin length, respectively. When two groins are symmetrically installed at both banks, the contraction caused by the groins increases the velocity in the main channel through the groin tips. As a result, the recirculation zone of symmetrical groins is slightly shorter than that of a single groin. When two groins are placed alternately, the backflow pattern behind Groin A presents three variation trends responding to the location of Groin B, which is characterized by a critical spacing equal to the groin length, i.e., 5 cm in the present study. Specifically, with the increase in spacing between groins over 5 cm, an upstream alternating Groin B promotes the development of the recirculation zone behind Groin A, whereas a downstream alternating Groin B inhibits the generation and propagation of reversing flow induced by Groin A. It implies that the threshold behavior of backflow patterns depends on the ratio of spacing between two groins to groin length in the alternate layout of short groins. For the short groin used in the study, the threshold value of the ratio is one.

Spanwise velocity near the groin tip, which is also located in the shear layer zone ($0.089 \text{ m/s} \geq v_{xy} \geq 0.030 \text{ m/s}$), was fitted as linearly related to the width of recirculation zone via correlation analysis. The spanwise velocity has a dominant effect on the width of the downstream recirculation zone from the angular performance of streamline curvature. Additionally, the variation of groin-induced vorticity and recirculation zone length remains almost constant with different spacing between groins.

Based on momentum conservation, considering and correcting the contraction ratio of cross-section between groins at both banks, dimensionless empirical formulas estimating the recirculation zone length of alternating groins are, respectively, derived corresponding to different spacing between groins. The coefficient of determination R^2 is over 0.99. It implies the results from the updated empirical formula can be considered conservative, first-order estimates of the recirculation length formed behind short groins placed in an alternating configuration.

This study enriches the knowledge on backflow features of two alternating groins with various spacing, which provides a scientific reference to assess the cumulative effect of a groin group in a natural river system. In addition, these findings will be useful for cost-effective configuration of short groins at both riverbanks with respect to optimizing navigation and flood prevention.

Author Contributions: Methodology, C.K., Y.Z., J.G.; formal analysis, C.K., Y.Z. and J.G.; investigation, Y.Z., J.G.; resources, J.G.; data curation, J.G.; visualization, Y.Z., X.H.; supervision, C.K.,

J.G.; writing—original draft preparation, C.K., Y.Z.; writing—review and editing, C.K., Q.Z.; project administration, C.K.; funding acquisition, C.K. All authors have read and agreed to the published version of the manuscript.

Funding: This research was funded by the National Natural Science Foundation of China, grant number 41776098 and 41976159 and the National Key Research and Development Project of China, grant number 2019YFC1407900.

Institutional Review Board Statement: Not applicable.

Informed Consent Statement: Not applicable.

Data Availability Statement: Data will be available under request to authors.

Conflicts of Interest: The authors declare no conflict of interest.

References

1. U.S. Army Corps of Engineers (USACE). *Coastal Groins and Nearshore Breakwaters*; U.S. Army Corps of Engineers: Washington, DC, USA, 1992.
2. Fazli, M.; Ghodsian, M.; Neyshabouri, S.A.A.S. Scour and flow field around a spur dike in a 90° bend. *Int. J. Sediment Res.* **2008**, *23*, 56–68. [CrossRef]
3. Ettema, R.; Muste, M. Scale effects in flume experiments on flow around spur dike in flatbed channel. *J. Hydraul. Eng.* **2004**, *130*, 635–646. [CrossRef]
4. Abhari, M.N.; Ghodsian, M.; Vaghefi, M.; Panahpur, N. Experimental and numerical simulation of flow in a 90° bend. *Flow Meas. Instrum.* **2010**, *21*, 292–298. [CrossRef]
5. Karami, H.; Ardeshir, A.; Behzadian, K.; Ghodsian, M. Protective spur dike for scour mitigation of existing spur dikes. *J. Hydraul. Res.* **2011**, *49*, 809–813. [CrossRef]
6. Koken, M.; Constantinescu, G. An investigation of the flow and scour mechanisms around isolated spur dikes in a shallow open channel: 2. Conditions corresponding to the final stages of the erosion and deposition process. *Water Resour. Res.* **2008**, *44*, W08407. [CrossRef]
7. Azinfar, H.; Kells, J.A. Flow resistance due to a single spur dike in an open channel. *J. Hydraul. Res.* **2009**, *47*, 755–763. [CrossRef]
8. Weitbrecht, V.; Kuhn, G.; Jirka, G.H. Large scale PIV-measurements at the surface of shallow water flows. *Flow Meas. Instrum.* **2002**, *13*, 237–245. [CrossRef]
9. Ohmoto, T.; Hirakawa, R.; Koreeda, N. Effects of water surface oscillation on turbulent flow in an open channel with a series of spur dikes. In Proceedings of the Hydraulic Measurements and Experimental Methods Specialty Conference (HMEM), Estes Park, CO, USA, 28 July–1 August 2002. [CrossRef]
10. Uijttewaal, W.S.J. Effects of groyne layout on the flow in groyne fields: Laboratory experiments. *J. Hydraul. Eng.* **2005**, *131*, 782–791. [CrossRef]
11. Kuhnle, R.A.; Jia, K.; Alonso, C.V. Measured and simulated flow near a submerged spur dike. *J. Hydraul. Eng.* **2008**, *134*, 916–924. [CrossRef]
12. Francis, J.R.D.; Pattanaik, A.B.; Wearne, S.H. Technical Note: Observations of flow patterns around some simplified groyne structures in channels. *ICE Proc.* **1968**, *41*, 829–837. [CrossRef]
13. Rajaratnam, N.; Nwachukwu, B.A. Flow near groin-like structures. *J. Hydraul. Eng.* **1983**, *109*, 463–480. [CrossRef]
14. Schmidt, J.C.; Rubin, D.M.; Ikeda, H. Flume simulation of recirculating flow and sedimentation. *Water Resour. Res.* **1993**, *29*, 2925–2939. [CrossRef]
15. Duan, J.G. Mean flow and turbulence around a laboratory. *J. Hydraul. Eng.* **2009**, *135*, 803–811. [CrossRef]
16. Molls, T.; Chaudhry, M.H.; Khan, K.W. Numerical simulation of two-dimensional flow near a spur-dike. *Adv. Water Resour.* **1995**, *18*, 227–236. [CrossRef]
17. Ouillon, S.; Dartus, D. Three-dimensional computation of flow around groyne. *J. Hydraul. Eng.* **1997**, *123*, 962–970. [CrossRef]
18. Peng, J.; Kawahara, Y. Application of linear and non-linear k-ε model to flows around spur dikes. *Ann. J. Hydraul. Eng.* **1998**, *42*, 643–648. [CrossRef]
19. Nagata, N.; Hosoda, T.; Nakato, T.; Muramot, Y. Three-dimensional numerical model for flow and bed deformation around river hydraulic structures. *J. Hydraul. Eng.* **2005**, *131*, 1074–1087. [CrossRef]
20. Noh, J.W.; Lee, S.J.; Kim, J.S.; Molinas, A. Numerical modeling of flow and scouring around a cofferdam. *J. Hydro-environ. Res.* **2012**, *6*, 199–309. [CrossRef]
21. Koken, M.; Constantinescu, G. An investigation of the dynamics of coherent structures in a turbulent channel flow with a vertical sidewall obstruction. *Phys. Fluids* **2009**, *21*, 085104. [CrossRef]
22. Higham, J.E.; Brevis, W.; Keylock, C.J.; Safarzadeh, A. Using modal decompositions to explain the sudden expansion of the mixing layer in the wake of a groyne in a shallow flow. *Adv. Water Resour.* **2017**, *107*, 451–459. [CrossRef]
23. Uijttewaal, W.S.J.; Lehmann, D.; van Mazijk, A. Exchange processes between a river and its groyne fields: Model experiments. *J. Hydraul. Eng.* **2001**, *127*, 928–936. [CrossRef]

24. Weitbrecht, V.; Jirka, G.H. Flow patterns and exchange processes in dead zones of rivers. In Proceedings of the 29th IAHR Congress, Beijing, China, 16–21 September 2001; pp. 439–455.
25. Sukhodolov, A.; Uijttewaal, W.S.J.; Engelhardt, C. On the correspondence between morphological and hydrodynamical patterns of groyne fields. *Earth Surf. Process. Landf.* **2002**, *27*, 289–305. [CrossRef]
26. Uijttewaal, W.S.J. The flow in groyne field. In *Water Quality Hazards and Dispersion of Pollutants*; Czernuszenko, W., Rowinski, P., Eds.; Springer: Warsaw, Poland, 2005. [CrossRef]
27. Yossef, M.F.M.; de Vriend, H.J. Flow details near river groynes: Experimental investigation. *J. Hydraul. Eng.* **2011**, *137*, 504–516. [CrossRef]
28. Uijttewaal, W.S.J. Hydrodynamics of shallow flows: Application to rivers. *J. Hydraul. Res.* **2014**, *52*, 157–172. [CrossRef]
29. Akkermans, R.A.D.; Clesilk, A.R.; Kamp, L.P.J.; Trieling, R.R.; Clercx, H.J.H.; van Heijst, G.J.F. The three-dimensional structure of an electromagnetically generated dipolar vortex in a shallow fluid layer. *Phys. Fluids* **2008**, *20*, 116601. [CrossRef]
30. Cieślik, A.R.; Akkermans, R.A.D.; Kamp, L.P.J.; Clercx, H.J.H.; van Heijst, G.J.F. Dipole-wall collision in a shallow fluid. *Eur. J. Mech. B Fluids* **2009**, *28*, 397–404. [CrossRef]
31. Van Heijst, G.J.F.; Clercx, H.J.H. Laboratory modeling of geophysical vortices. *Annu. Rev. Fluid Mech.* **2009**, *41*, 143–164. [CrossRef]
32. Akkermans, R.A.D.; Kamp, L.P.J.; Clercx, H.J.H.; van Heijst, G.J.F. Three-dimensional flow in electromagnetically driven shallow two-layer fluids. *Phys. Rev. E* **2010**, *82*, 026314. [CrossRef]
33. McCoy, A.; Constantinescu, G.; Weber, L. Coherent structures and mass exchange processes in channel flow with spanwise obstructions. In Proceedings of the ERCOFTAC International Symposium on Engineering Turbulence Modelling and Measurements, ETMM6, Sardinia, Italy, 23–25 May 2005; IIHR-Hydroscience and Engineering, Department of Civil and Environmental Engineering, The University of Iowa: Iowa City, IA, USA, 2005. [CrossRef]
34. Ahmed, H.S.; Hasan, M.M.; Tanaka, N. Analysis of flow around impermeable groynes on one side of symmetrical compound channel: An experimental study. *Water Sci. Eng.* **2010**, *3*, 56–66. [CrossRef]
35. McCoy, A.; Constantinescu, G.; Weber, L.J. Numerical Investigation of Flow Hydrodynamics in a Channel with a Series of Groynes. *J. Hydraul. Eng.* **2008**, *134*, 157–172. [CrossRef]
36. Fang, H.W.; Bai, J.; He, G.J.; Zhao, H.M. Calculations of nonsubmerged groin flow in a shallow open channel by Large-Eddy Simulation. *J. Eng. Mech.* **2014**, *140*, 04014016. [CrossRef]
37. Koutrouveli, T.L.; Dimas, A.A.; Fourniotis, N.T.H.; Demetracopoulos, A.C. Groyne spacing role on the effective control of wall shear stress in open-channel flow. *J. Hydraul. Res.* **2019**, *57*, 167–182. [CrossRef]
38. Ning, J.; Li, G.; Li, S. Numerical simulation of the influence of spur dikes spacing on local scour and flow. *Appl. Sci.* **2019**, *9*, 2306. [CrossRef]
39. Gu, Z.P.; Ikeda, S. Experimental study of open channel flow with groins. In Proceedings of the 16th IAHR-APD Congress and 3rd Symposium of IAHR-ISHS 2009, Nanjing, China, 20–23 October 2008; pp. 1951–1956. [CrossRef]
40. Cao, X.M.; Gu, Z.H.; Tang, H.W. Study on spacing threshold of nonsubmerged spur dikes with alternate layout. *J. Appl. Math.* **2013**, *2013*, 945984. [CrossRef]
41. Krishna, P.S.; Indulekha, K.P.; Balan, K. Analysis of groyne placement on minimizing river bank erosion. *Procedia Technol.* **2016**, *24*, 47–53. [CrossRef]
42. Cuong, T.V.; Hung, N.T.; Te, V.T.; Tuan, P.A. Analysis of spur dikes spatial layout to river bed degradation under reversing tidal flow. In Proceedings of the 10th International Conference on Asian and Pacific Coasts (APAC 2019), Hanoi, Vietnam, 25–28 September 2019. [CrossRef]
43. Mostafaa, M.M.; Ahmeda, H.S.; Ahmed, A.A.; Abdel-Raheeme, G.A.; Ali, N.A. Experimental study of flow characteristics around floodplain single groyne. *J. Hydro-Environ. Res.* **2019**, *22*, 1–13. [CrossRef]
44. Shields, F.D. Fate of Lower Mississippi River habitats associated with river training dikes. *Aquat. Conserv.* **1995**, *5*, 97–108. [CrossRef]
45. Jamieson, E.C.; Rennie, C.D. 3-D flow and scour near a submerged wing dike: ADCP measurements on the Missouri River. *Water Resour. Res.* **2011**, *47*, W07544. [CrossRef]
46. Braun, A.P.; Sobotka, M.J.; Phelps, Q.E. Fish Associations among Un-notched, Notched and L-head Dikes in the Middle Mississippi River. *River Res. Appl.* **2016**, *32*, 804–811. [CrossRef]
47. Ten Brinke, W.B.M.; Schulze, F.H.; Van der Veer, P. Sand exchange between groyne-field beaches and the navigation channel of the Dutch Rhine: The impact of navigation versus river flow. *River Res. Appl.* **2004**, *20*, 899–928. [CrossRef]
48. Sieben, J. Sediment management in the Dutch Rhine branches. *Int. J. River Basin Manag.* **2009**, *7*, 43–53. [CrossRef]
49. Arnaud, F.; Schmitt, L.; Johnstone, K.; Rollet, A.J.; Piégay, H. Engineering impacts on the Upper Rhine channel and floodplain over two centuries. *Geomorphology* **2019**, *330*, 13–27. [CrossRef]
50. Wu, C.P.; Qi, P.; Zhang, L.Z.; Guo, H.M.; Chen, J.J.; Guo, Z.L. Test and Study on Banks Regulation Model of Wandering Section in the Lower Yellow River. *Yellow River* **2005**, *27*, 12–19. (In Chinese)
51. Liu, Y.; Wang, B.M.; Li, Y.Q. Research on application of removable non-rescue submerged groins in lower Yellow River training works. *Procedia Eng.* **2012**, *28*, 781–785. [CrossRef]
52. Zhang, L.; Wu, B.F.; Yin, K.; Li, X.S.; Kia, K.; Zhu, L. Impacts of human activities on the evolution of estuarine wetland in the Yangtze Delta from 2000 to 2010. *Environ. Earth Sci.* **2015**, *73*, 435–447. [CrossRef]

53. Deng, Y.; Cao, M.X.; Ma, A.X.; Hu, Y.; Chang, L.H. Mechanism study on the impacts of hydraulic alteration on fish habitat induced by spur dikes in a tidal reach. *Ecol. Eng.* **2019**, *134*, 78–92. [CrossRef]
54. Jiao, J.; Dou, X.P.; Gao, X.Y.; Ding, L.; Yang, X.Y. Morphodynamic characteristics and medium-term simulation of the North−South Passage under the impact of the Yangtze Estuary deepwater navigation channel project. *China Ocean Eng.* **2020**, *34*, 198–209. [CrossRef]
55. Yossef, M.F.M. *The Effect of Groynes on Rivers: Literature Review*; Delft Cluster Project No.03.03.04 2002; Delft University of Technology: Delft, The Netherlands, 2002. Available online: http://resolver.tudelft.nl/uuid:b9545ba7-2423-4c20-ace2-0e1cd799d18a (accessed on 23 August 2002).
56. Bahrami-Yarahmadi, M.; Pagliarab, S.; Yabarehpourc, E.; Najafic, N. Study of Scour and Flow Patterns around Triangular-Shaped Spur Dikes. *KSCE J. Civ. Eng.* **2020**, *24*, 3279–3288. [CrossRef]
57. Xu, Y.; Zhang, Y.Y.; Nicolleau, F.C.G.A.; Wang, Z.C. PIV of swirling flow in a conical pipe with vibrating wall. *Int. J. Appl. Mech.* **2018**, *10*, 1850022. [CrossRef]
58. Zhang, L.; Shan, X.B.; Xie, T. Enhancing flow field performance of a small circulating water channel based on porous grid plate. *Appl. Sci.* **2020**, *10*, 5103. [CrossRef]
59. Sterczyńska, M.; Jakubowski, M. Research on particles' velocity distribution in a whirlpool separator using the PIV method of measurement. *Int. J. Food Eng.* **2017**, *13*, 0316. [CrossRef]
60. Sterczyńska, M.; Stachnik, M.; Poreda, A.; Piepiórka-Stepuk, J.; Zdaniewicz, M.; Jakubowski, M. The improvement of flow conditions in a whirlpool with a modified bottom: An experimental study based on particle image velocimetry (PIV). *J. Food Eng.* **2021**, *289*, 110164. [CrossRef]
61. Dou, G.R.; Chai, T.S.; Fan, M. An investigation on the whirlpool flow and its similarity laws. *Hydro-Sci. Eng.* **1978**, *3*, 1–24. (In Chinese)